$\tilde{\tau}_1$ lightest supersymmetric particle phenomenology: Two- versus four-body decay modes and resonant single slepton production at the LHC as an example

H. K. Dreiner* and S. Grab†

Bethe Center for Theoretical Physics & Physikalisches Institut der Universität Bonn, Nußallee 12, 53115 Bonn, Germany

M. K. Trenkel‡

Max-Planck-Institut für Physik, Föhringer Ring 6, 80805 München, Germany

(Received 8 September 2008; published 13 January 2009; publisher error corrected 15 January 2009)

We investigate B_3 minimal supergravity models, where the lightest stau $\tilde{\tau}_1$ is the lightest supersymmetric particle. B_3 models allow for lepton number and R-parity violation; the lightest supersymmetric particle can thus decay. We assume one nonzero B_3 coupling λ'_{ijk} at $M_{\rm GUT}$, which generates further B_3 couplings at M_Z. We study the renormalization group equations and give numerical examples. The new couplings lead to additional $\tilde{\tau}_1$ decays, providing distinct collider signatures. We classify the $\tilde{\tau}_1$ decays and describe their dependence on the minimal supergravity parameters. We exploit our results for single slepton production at the LHC. As an explicit numerical example, we investigate single-smuon production, focussing on like-sign dimuons in the final state. Also considered are final states with three or four muons.

DOI: 10.1103/PhysRevD.79.016002 PACS numbers: 11.10.Hi, 04.65.+e, 12.60.Jv, 14.80.Ly

I. INTRODUCTION

Supersymmetry [1–4] (SUSY) is one of the most promising extensions of the standard model (SM) of particle physics [5,6]. In its simplest form, we obtain the supersymmetric standard model (SSM), with a doubling of the SM particle content and one extra Higgs doublet. The SSM solves the hierarchy problem of the SM if SUSY is broken at a mass scale $\lesssim \mathcal{O}(10\ \text{TeV})$. Therefore, SUSY should be testable at the LHC [7,8], which will start taking data this year.

If they exist, supersymmetric particles are typically much heavier than their SM partners and at colliders will mostly decay rapidly. This leads to cascade decay chains in the detector to the lightest supersymmetric particle (LSP). The nature of the LSP and its possible decay modes is thus an essential feature for all supersymmetric signatures. It is the purpose of this paper to study a novel supersymmetric phenomenology, namely, with the lightest scalar tau (stau) $\tilde{\tau}_1$ as the LSP [9,10]. In particular we analyze in detail the potential $\tilde{\tau}_1$ decays in baryon-triality B_3 models [11–15]. We then study the discovery potential of a specific signature in this framework, namely, resonant single slepton production at the LHC, resulting in multiple muons in the final state.

A. The B_3 framework

The most general renormalizable superpotential of the SSM is [16,17]

$$W_{\rm SSM} = W_{\rm P_6} + W_{\not{\rm P}_6}, \tag{1.1}$$

$$W_{\rm P_6} = \epsilon_{ab}[(\mathbf{Y}_E)_{ij} L_i^a H_d^b \bar{E}_j + (\mathbf{Y}_D)_{ij} Q_i^{ax} H_d^b \bar{D}_{jx} + (\mathbf{Y}_U)_{ij} Q_i^{ax} H_u^b \bar{U}_{jx} + \mu H_d^a H_u^b], \tag{1.2}$$

$$W_{\not{\rm P}_6} = \epsilon_{ab}\left[\frac{1}{2}\lambda_{ijk} L_i^a L_j^b \bar{E}_k + \lambda'_{ijk} L_i^a Q_j^{bx} \bar{D}_{kx}\right] + \epsilon_{ab}\kappa^i L_i^a H_u^b + \frac{1}{2}\epsilon_{xyz}\lambda''_{ijk}\bar{U}_i^x \bar{D}_j^y \bar{D}_k^z. \tag{1.3}$$

Here, we use the standard notation of Ref. [18].

The superpotential (1.1) consists of two different parts. $W_{\rm P_6}$, involves the lepton $\mathbf{Y}_E$, down-quark $\mathbf{Y}_D$, and up-quark $\mathbf{Y}_U$ Yukawa matrices, which give mass to the leptons and quarks after electroweak symmetry breaking.

$W_{\not{\rm P}_6}$, consists of lepton and baryon number violating operators, which together can lead to rapid proton decay [19–22]. The SSM thus requires an additional symmetry [11,12,14] to stabilize the proton. The most widely assumed symmetry is R-parity, which prohibits $W_{\not{\rm P}_6}$, leading to the MSSM. But R-parity allows dangerous dimension-five proton decay operators such as $QQQL$ [23], thus proton-hexality P_6 is preferred [14]. Here, we consider a third possibility, baryon-triality B_3. B_3 is a discrete $\mathbf{Z}_3$ symmetry that prohibits only the $\bar{U}\bar{D}\bar{D}$ operators in Eq. (1.3) but also the dangerous dimension-five operators. See, for example, Refs. [24–26] for B_3 models that provide a dark matter candidate.

The B_3 SSM has some distinguishing features compared to the MSSM [21,27], which can have a strong impact on (hadron) collider phenomenology [28,29]:

(1) Lepton flavor and lepton number are violated.

*dreiner@th.physik.uni-bonn.de
†sgrab@th.physik.uni-bonn.de
‡trenkel@mppmu.mpg.de

(2) The renormalization group equations (RGEs) get additional contributions [10,30,31].
(3) Neutrino masses can be generated as experimentally observed [32–37].
(4) The LSP is not stable.
(5) Supersymmetric particles can be produced singly, possibly on resonance.

Since the LSP is not stable, we are not restricted to the lightest neutralino $\tilde{\chi}_1^0$ as the LSP [38]. The most general B_3 SSM has more than 200 parameters and in principle any SUSY particle can be the LSP. Within the MSSM, the most widely studied constrained model is minimal supergravity (mSUGRA) with conserved P_6 and radiative electroweak symmetry breaking [39–43]. The 124 free parameters of the MSSM are reduced to only five

$$M_0, \quad M_{1/2}, \quad A_0, \quad \tan\beta, \quad \mathrm{sgn}(\mu), \tag{1.4}$$

which are fixed at the grand unification (GUT) scale, M_{GUT}. We have a universal scalar mass M_0, a universal gaugino mass $M_{1/2}$, a universal trilinear scalar coupling A_0, the ratio of the Higgs vacuum expectation values $\tan\beta$, and the sign of the Higgs mixing parameter $\mathrm{sgn}(\mu)$. For a wide range of these parameters a $\tilde{\chi}_1^0$ LSP is in fact obtained at the weak scale M_Z [44]. There are also wide ranges of parameter space with a $\tilde{\tau}_1$ LSP, but these are cosmologically excluded in the MSSM or mSUGRA [38].

In the B_3 mSUGRA model we consider here [9,10], we have six parameters at the GUT scale

$$M_0, \quad M_{1/2}, \quad A_0, \quad \tan\beta, \quad \mathrm{sgn}(\mu), \quad \text{and} \quad \Lambda', \tag{1.5}$$

where Λ' stands for one nonvanishing coupling λ'_{ijk}. A first investigation of the parameter space has shown, that there are extensive regions with a neutralino, a stau or a sneutrino LSP [9,10]. We shall focus here on a $\tilde{\tau}_1$ LSP. $\tilde{\tau}_1$ LSP scenarios have been studied in the literature [9,10,37,45–51]. As we now discuss, we go beyond this work in several aspects.

B. New phenomenology and outline

The $\tilde{\tau}_1$ LSP might decay via the dominant $L_iQ_j\bar{D}_k$ operator, Eq. (1.3); for example, via a 4-body decay in the presence of a nonvanishing λ'_{211}

$$\tilde{\tau}_1^- \xrightarrow{\lambda'_{211}} \tau^- \mu^- u \bar{d}. \tag{1.6}$$

An important feature of B_3 mSUGRA models is that additional B_3 couplings are generated via the RGE running. These new couplings can lead to 2-body decays of the $\tilde{\tau}_1$ LSP. For example, λ'_{211} will generate λ_{233}, which allows for the decay

$$\tilde{\tau}_1^- \xrightarrow{\lambda_{233}} \mu^- \nu_\tau. \tag{1.7}$$

Even though $\lambda_{233} \ll \lambda'_{211}$, this might be the dominant decay mode. The decay (1.6) is suppressed by phase space and heavy propagators.

We analyze in detail the conditions for a dominance of the 2-body decay over the 4-body decay. We provide for the first time an extensive study of B_3 $\tilde{\tau}_1$ LSP decays and extend and specify thus the results of [51], where a first estimate has been performed. This is useful when studying both pair produced and singly produced SUSY particles within the B_3 mSUGRA model. Typically, all heavy SUSY particle decay to the $(\tilde{\tau}_1)$ LSP.

In the second half of our paper, we consider the B_3 mSUGRA model with a $\tilde{\tau}_1$ LSP and focus on resonant single (left-handed) charged slepton $\tilde{\ell}_{Li}$ and sneutrino $\tilde{\nu}_i$ production at hadron colliders, which proceeds via a dominant $L_iQ_j\bar{D}_k$ operator

$$\bar{u}_j d_k \xrightarrow{\lambda'_{ijk}} \tilde{\ell}_{Li}^-, \tag{1.8}$$

$$\bar{d}_j d_k \xrightarrow{\lambda'_{ijk}} \tilde{\nu}_i. \tag{1.9}$$

Here, u_j (d_k) is an up-type (down-type) quark of generation j (k).

Single slepton production allows us also to study two B_3 couplings at a time, depending on the scenario. The slepton is always produced via a λ', whereas the decay of the $\tilde{\tau}_1$ LSP in the decay chain of the slepton might proceed via a generated λ, cf. Eq. (1.7).

Single slepton production within a $\tilde{\chi}_1^0$ LSP scenario leads to like-sign dileptons in the final state and has thus a very promising signature for experimental studies, see Refs. [52–56]. Here, we show that for a $\tilde{\tau}_1$ LSP, we also obtain like-sign dilepton events and additionally events with three or four leptons in the final state. We give event rates for the LHC for two representative sets of B_3 mSUGRA parameters. We also discuss the background, although a detailed signal over background analysis is beyond the scope of this paper. This is the first study of single slepton production in $\tilde{\tau}_1$ LSP scenarios.

We assume in the following that only one nonvanishing λ'_{ijk} is present at M_{GUT}, similar to the dominant top Yukawa in the SM. Allowing for more than one coupling leads to stricter bounds [18,21,27,57–59]. The bounds for a single λ'_{ijk} lie between $\mathcal{O}(1)$ and $\mathcal{O}(10^{-4})$ depending on the flavor indices and sparticle masses. These bounds can be up to 4 orders of magnitude stronger at M_{GUT} if one includes the generation of neutrino masses [10,18]. We therefore assume below that $\lambda'_{ijk} \lesssim \mathcal{O}(10^{-2})$ and require it to be consistent with the observed neutrino masses.

Resonant slepton production at hadron colliders via the $L_iQ_j\bar{D}_k$ operator was first investigated in [60,61], using tree-level production cross sections. Three-lepton final states and like-sign dilepton events were investigated in Refs. [52–56]. Ref. [62] considered scenarios with a gravitino LSP. Experimental studies by the D0 collaboration at the Tevatron were performed in Refs. [63,64] assuming a $\tilde{\chi}_1^0$ LSP and a nonvanishing λ'_{211}. The next-to-leading order (NLO) QCD corrections to the cross section were com-

puted in [65–68]. The SUSY-QCD corrections were included by [67]. The latter can modify the NLO QCD prediction by up to 35%. In Refs. [50,69–71] single slepton production in association with a single top quark was considered.

The outline of our paper is as follows: In Sec. II, we review the B_3 mSUGRA model and approximate formulæ for sparticle masses. We define two B_3 mSUGRA scenarios with a $\tilde{\tau}_1$ LSP, as a reference for phenomenological studies. We then derive approximate equations for the RGE generation of λ from λ'. In Sec. III, we classify the different decay modes of the $\tilde{\tau}_1$ LSP and investigate the conditions for a dominance of the 2-body decay over the 4-body decay and *vice versa*. In Sec. IV, we classify all possible signatures for resonant single slepton production in B_3 mSUGRA models with a $\tilde{\tau}_1$ LSP. In Sec. V, we calculate event rates for like-sign dimuon events as well as for three- and four-muon events, at the LHC. We also discuss backgrounds and cuts for like-sign dimuon events. We conclude in Sec. VI.

II. THE LOW ENERGY SPECTRUM OF THE B_3 MSUGRA MODEL WITH A $\tilde{\tau}_1$ LSP

We have defined the B_3 mSUGRA model in Eq. (1.5) via six input parameters at the GUT scale [9,10]. We now discuss the low energy spectrum. Sparticle masses and couplings are obtained by running the respective RGEs down to the weak scale. Because of the mixing of different quark flavors, described by the Cabibbo-Kobayashi-Maskawa (CKM) matrix, the RGEs of the B_3 couplings are not independent, but highly coupled. Therefore, a single nonzero λ'_{ijk} at the GUT scale generates a set of other nonzero B_3 couplings at lower scales. Assuming a diagonal charged lepton Yukawa matrix $\mathbf{Y}_E$, only those couplings can be generated that violate the same lepton number as λ'_{ijk}, i.e. λ'_{imn} and λ_{ill}. No additional source of lepton number violation is introduced. Phenomenologically particularly relevant is the generation of λ_{i33}, which we discuss in detail in Sec. II D.

A. Sparticle spectra

The low energy SUSY particle masses depend strongly on the universal mSUGRA parameters (1.4) and only weakly on $\lambda' \lesssim \mathcal{O}(10^{-2})$ [9]. For later use, we cite here approximate expressions for the relevant SUSY particle masses in terms of the mSUGRA parameters as given in [72], cf. also the original work in Ref. [44]. The masses of the sleptons of the first and second generation are

$$\begin{aligned} m^2_{\tilde{\ell}_R} &= M_0^2 + 0.15 M_{1/2}^2 - \sin^2\theta_W M_Z^2 \cos 2\beta, \\ m^2_{\tilde{\ell}_L} &= M_0^2 + 0.52 M_{1/2}^2 - (0.5 - \sin^2\theta_W) M_Z^2 \cos 2\beta, \\ m^2_{\tilde{\nu}} &= M_0^2 + 0.52 M_{1/2}^2 + 0.5 M_Z^2 \cos 2\beta, \end{aligned} \tag{2.1}$$

where $m_{\tilde{\ell}_{R,L}}$ denotes the mass of a right-/left-handed selectron or smuon, respectively, $m_{\tilde{\nu}}$ the mass of a left-handed electron or muon sneutrino, and θ_W the electroweak mixing angle. M_Z is the mass of the Z boson.

For sfermions of the third generation, the mixing between left- and right-handed gauge-current eigenstates has to be taken into account. The stau mass matrix squared $\mathfrak{M}^2_{\tilde{\tau}}$ is given by [73]

$$\mathfrak{M}^2_{\tilde{\tau}} = \begin{pmatrix} m_\tau^2 + A_{LL} & m_\tau B_{LR} \\ m_\tau B_{LR} & m_\tau^2 + C_{RR} \end{pmatrix}, \tag{2.2}$$

with m_τ denoting the tau lepton mass and, expressed in terms of left- and right-handed third-generation softbreaking parameters $m_{\tilde{L}_3}$ and $m_{\tilde{E}_3}$, respectively,

$$\begin{aligned} A_{LL} &= m^2_{\tilde{L}_3} - (0.5 - \sin^2\theta_W) M_Z^2 \cos 2\beta, \\ B_{LR} &= A_\tau - \mu \tan\beta, \\ C_{RR} &= m^2_{\tilde{E}_3} - \sin^2\theta_W M_Z^2 \cos 2\beta, \end{aligned} \tag{2.3}$$

where A_τ is the trilinear coupling of the left- and right-handed stau to the Higgs. In mSUGRA, $A_\tau = A_0$ at the GUT scale. The softbreaking parameters depend on the mSUGRA parameters as follows [72]:

$$\begin{aligned} m^2_{\tilde{E}_3} &= M_0^2 + 0.15 M_{1/2}^2 - \frac{2}{3} X_\tau, \\ m^2_{\tilde{L}_3} &= M_0^2 + 0.52 M_{1/2}^2 - \frac{1}{3} X_\tau, \\ X_\tau &\equiv 10^{-4}(1 + \tan^2\beta)(M_0^2 + 0.15 M_{1/2}^2 + 0.33 A_0^2), \end{aligned} \tag{2.4}$$

where X_τ parameterizes the influence of the tau Yukawa coupling. Note, that X_τ can have a strong impact on the stau masses due to its $\tan^2\beta$ dependence, even though X_τ is suppressed by a factor 10^{-4}. We will investigate this effect on the $\tilde{\tau}_1$ decay branching ratios in the next section.

The stau mass eigenstates $\tilde{\tau}_{1,2}$ are obtained from the gauge eigenstates by a unitary rotation U such that U diagonalizes the mass matrix, $U\mathfrak{M}^2_{\tilde{\tau}}U^\dagger = \mathrm{diag}(m^2_{\tilde{\tau}_1}, m^2_{\tilde{\tau}_2})$, yielding for the masses $m_{\tilde{\tau}_{1,2}}$

$$\begin{aligned} m^2_{\tilde{\tau}_{1,2}} = m_\tau^2 &+ \frac{1}{2}(A_{LL} + C_{RR}) \\ &\mp \frac{1}{2}\sqrt{(A_{LL} - C_{RR})^2 + 4 m_\tau^2 B_{LR}^2}. \end{aligned} \tag{2.5}$$

The gaugino masses can be approximated in terms of the universal gaugino mass $M_{1/2}$ [72],

$$m_{\tilde{\chi}^0_1} \simeq M_1 = 0.41 M_{1/2}, \qquad m_{\tilde{\chi}^0_2} \simeq M_2 = 0.84 M_{1/2}. \tag{2.6}$$

Here, it has been used that the lightest neutralino $\tilde{\chi}^0_1$ is binolike in many mSUGRA models and that its mass can be approximated by the bino mass parameter M_1 at the weak scale. Accordingly, the second lightest neutralino $\tilde{\chi}^0_2$ is mainly winolike, and its mass governed by the wino mass parameter M_2.

B. Reference scenarios with a $\tilde{\tau}_1$ LSP

For the purpose of numerical studies and as future reference points, we define two specific sets of B_3 mSUGRA scenarios with a $\tilde{\tau}_1$ LSP

$$\begin{aligned}
&\text{Set A: } M_0 = 0 \text{ GeV}, && M_{1/2} = 500 \text{ GeV},\\
&A_0 = 600 \text{ GeV}, && \tan\beta = 13,\\
&\operatorname{sgn}(\mu) = +1, && \text{a single } \lambda'_{ijk} \neq 0|_{\text{GUT}},\\
&\text{Set B: } M_0 = 0 \text{ GeV}, && M_{1/2} = 700 \text{ GeV},\\
&A_0 = 1150 \text{ GeV}, && \tan\beta = 26,\\
&\operatorname{sgn}(\mu) = +1, && \text{a single } \lambda'_{ijk} \neq 0|_{\text{GUT}}.
\end{aligned} \tag{2.7}$$

They are chosen in accordance with the following bounds [106]:

(i) $\mathrm{BR}(B_s \to \mu^+\mu^-) < 5.8 \times 10^{-8}$ at the 95% C.L. obtained by the CDF Collaboration [74].

(ii) $2.76 \times 10^{-4} < \mathrm{BR}(b \to s\gamma) < 4.34 \times 10^{-4}$, which is the central theoretical value at 2σ [9] using the experimental value of [75].

(iii) The discrepancy between experiment and the SM prediction of the anomalous magnetic moment of the muon is $\delta a_\mu = a_\mu^{\text{exp}} - a_\mu^{\text{SM}} = (29.5 \pm 8.8) \times 10^{-10}$, i.e. 3.4σ [76–78]. The sets (2.7) are chosen such that $\delta a_\mu^{\text{SUSY}} = a_\mu^{\text{MSSM}} - a_\mu^{\text{SM}}$ agrees with δa_μ within 2σ.

(iv) Higgs mass $m_{h^0} \geq 112.4$ GeV. This value corresponds to the LEPII bound of $m_{h^0} \geq 114.4$ GeV at 95% C.L. [79] assuming a numerical error of 2 GeV for the mass prediction.

(v) A nonvanishing coupling λ'_{ijk} at the GUT scale will generate a tree-level neutrino mass [10,32,80–82]. All couplings λ'_{ijk} in the following are chosen such that the tree-level neutrino mass is smaller than the cosmological bound on the sum of neutrino masses from the Wilkinson Microwave Anistropy Probe [83] combined with 2dGRFS data [84]: $\sum_i m_{\nu_i} < 0.71$ eV. A corresponding comprehensive set of bounds for the mSUGRA parameter set SPS1a [85] with one nonvanishing coupling λ'_{ijk} is given in Ref. [10]. Note, that the generated tree-level neutrino mass depends on all mSUGRA parameters (1.5). The neutrino mass bounds on λ'_{ijk} for Set A and Set B are weaker compared to those for SPS1a.

We use the computer programs provided by [86–88] to calculate $\mathrm{BR}(B_s \to \mu^+\mu^-)$, $\mathrm{BR}(b \to s\gamma)$, and $\delta a_\mu^{\text{SUSY}}$. These programs do not include the B_3 couplings. But the corresponding effects are negligible for $\lambda'_{ijk} \lesssim \mathcal{O}(10^{-2})$ [9].

We show in Table I the supersymmetric mass spectra of the parameter Sets A and B (2.7). We have neglected the mass dependence on the different nonzero B_3 couplings, which is valid if $\lambda'_{ijk} \lesssim \mathcal{O}(10^{-2})$ [9]. The main B_3 effect on the spectrum is that we allow for a $\tilde{\tau}_1$ LSP.

TABLE I. Sparticle masses for the B_3 mSUGRA Sets A and B as defined in Eq. (2.7), evaluated for a renormalization scale $Q_{\text{susy}} = \sqrt{m_{\tilde{t}_1}(Q_{\text{susy}}) m_{\tilde{t}_2}(Q_{\text{susy}})}$ using SOFTSUSY 2.0.10 [89]. The variation due to different $\lambda'_{ijk} \neq 0|_{\text{GUT}}$ and quark mixing (see Sec. II C) is below the percent level. The masses in the second generation coincide with those in the first generation.

	Masses [GeV]			Masses [GeV]	
	Set A	Set B		Set A	Set B
$\tilde{\tau}_1$	179	146	$\tilde{\chi}_1^0$	203	290
$\tilde{e}_R$	193	266	$\tilde{\chi}_2^0$	380	544
$\tilde{\tau}_2$	340	453	$\tilde{\chi}_3^0$	571	754
$\tilde{e}_L$	340	471	$\tilde{\chi}_4^0$	587	765
$\tilde{\nu}_\tau$	326	437	$\tilde{\chi}_1^\pm$	383	549
$\tilde{\nu}_e$	329	461	$\tilde{\chi}_2^\pm$	583	761
$\tilde{t}_1$	841	1160	h^0	113	115
$\tilde{b}_1$	970	1300	H^0	643	795
$\tilde{u}_R$	1010	1370	A^0	642	795
$\tilde{t}_2$	1010	1340	H^+	648	799
$\tilde{b}_2$	995	1340			
$\tilde{u}_L$	1040	1410	$\tilde{g}$	1150	1560

One naturally obtains a $\tilde{\tau}_1$ LSP spectrum for $M_{1/2} \gg M_0$. The large $M_{1/2}$ raises the lightest neutralino mass (2.6) faster than the right-handed slepton masses (2.1). It also drives the gluino and indirectly via the RGEs the squark masses up. We thus see in Table I squark and gluino masses $\gtrsim 1$ TeV, while the slepton masses are below 500 GeV. Another general feature of a $\tilde{\tau}_1$ LSP scenario is that the second lightest neutralino and the lightest chargino are also heavier than the sleptons. Therefore, the only conventional supersymmetric decays of the left-handed sleptons are via the lightest neutralino. Depending on the dominant B_3 coupling and its size, the left-handed sleptons can also decay into two jets.

Nearly all sparticles in Set B ($M_{1/2} = 700$ GeV) are heavier than in Set A ($M_{1/2} = 500$ GeV). The most important difference for the phenomenology at colliders arises from the different values of $\tan\beta$ ($\tan\beta = 13$ in Set A, $\tan\beta = 26$ in Set B). According to Eq. (2.4), the soft breaking parameters of the stau decrease for increasing $\tan\beta$ and thus both stau mass eigenstates are reduced for large values of $\tan\beta$. Furthermore, the mass of the lighter stau is reduced due to the larger L–R mixing, cf. Eq. (2.2). This effect can be seen in Table I, where the mass of the $\tilde{\tau}_1$ LSP is 179 GeV in Set A but only 146 GeV in Set B. The $\tilde{\tau}_1$ mass and $\tan\beta$ strongly influence the possible 2- and 4-body $\tilde{\tau}_1$ LSP branching ratios. We will investigate this topic in detail in Sec. III.

C. Fermion mixing

Since the B_3 RGEs are coupled, given one nonzero B_3 coupling at M_{GUT}, we will generate many nonzero cou-

plings at the weak scale M_Z. As we will see in the next section, the size of the dynamically generated B_3 couplings depends sensitively on the composition of the quark Yukawa matrices. For this reason we prepend here a short discussion of quark mixing in B_3 models.

Initially at $M_{\rm GUT}$, all parameters are given in the weak-current eigenstate basis. This includes the quark and lepton Yukawa coupling matrices $\mathbf{Y}_U$, $\mathbf{Y}_D$, $\mathbf{Y}_E$, and the corresponding mass matrices $\mathbf{m_u}$, $\mathbf{m_d}$, $\mathbf{m_e}$. Since, in general, these matrices are not diagonal, we need to rotate the (charged) lepton and quark fields from the weak into the mass eigenstate basis

$$f_{L,R}^{\rm mass} = \mathbf{V_{fL,R}} f_{L,R}^{\rm weak}, \tag{2.8}$$

with $f_{L,R}$ denoting the left- and right-handed fermion fields, respectively, and $\mathbf{V_{fL,R}}$ denoting the corresponding rotation matrices. The mass matrices in the mass eigenstate basis are then given by

$$\begin{aligned} \mathbf{V_{uL}} \mathbf{m_u} \mathbf{V_{uR}^+} &= \mathrm{diag}(m_u, m_c, m_t), \\ \mathbf{V_{dL}} \mathbf{m_d} \mathbf{V_{dR}^+} &= \mathrm{diag}(m_d, m_s, m_b), \\ \mathbf{V_{eL}} \mathbf{m_e} \mathbf{V_{eR}^+} &= \mathrm{diag}(m_e, m_\mu, m_\tau), \end{aligned} \tag{2.9}$$

defined at the weak scale M_Z. The rotation matrices $\mathbf{V_{fL,R}}$ are not directly experimentally accessible but only the CKM matrix $\mathbf{V_{CKM}}$,

$$\mathbf{V}_{\rm CKM} = \mathbf{V_{uL}} \mathbf{V_{dL}^+}. \tag{2.10}$$

In general, the rotation matrices for the left-handed fields differ from those for the right-handed fields. In the following, however, for simplicity and definiteness, we assume real and symmetric Yukawa coupling matrices, thus $\mathbf{V_{fL}} = \mathbf{V_{fR}}$. Furthermore, we neglect neutrino masses in this context and assume that $\mathbf{Y}_E$ is diagonal in the weak-current basis. Correspondingly, $\mathbf{V_{eL,R}} = \mathbf{1}_{3\times 3}$.

To further constrain the quark Yukawa couplings, we restrict ourselves to the extreme cases of quark mixing taking place completely in the up- or the down-quark sector, respectively. We will refer to it as ''up-type mixing'' if

$$\mathbf{V_{uL,R}} = \mathbf{V}_{\rm CKM}, \qquad \mathbf{V_{dL,R}} = \mathbf{1}_{3\times 3} \tag{2.11}$$

at the weak scale M_Z and as ''down-type mixing'' if

$$\mathbf{V_{uL,R}} = \mathbf{1}_{3\times 3}, \qquad \mathbf{V_{dL,R}} = \mathbf{V_{CKM}^+} \tag{2.12}$$

at the weak scale. Therefore, in up-type mixing scenarios, the Yukawa matrices are

$$\begin{aligned} \mathbf{Y}_U(M_Z) \times v_u &= \mathbf{V_{CKM}^+} \cdot \mathrm{diag}(m_u, m_c, m_t) \cdot \mathbf{V}_{\rm CKM}, \\ \mathbf{Y}_D(M_Z) \times v_d &= \mathrm{diag}(m_d, m_s, m_b), \end{aligned} \tag{2.13}$$

and in down-type mixing scenarios, the Yukawa matrices are

$$\begin{aligned} \mathbf{Y}_U(M_Z) \times v_u &= \mathrm{diag}(m_u, m_c, m_t), \\ \mathbf{Y}_D(M_Z) \times v_d &= \mathbf{V}_{\rm CKM} \cdot \mathrm{diag}(m_d, m_s, m_b) \cdot \mathbf{V_{CKM}^+}, \end{aligned} \tag{2.14}$$

respectively. In the following, we will consider these two extreme cases. v_u (v_d) is the vacuum expectation value of the up-type (down-type) neutral CP-even Higgs with

$$v_u = v \sin\beta, \qquad v_d = v \cos\beta, \tag{2.15}$$

where $v = 174$ GeV is the SM vacuum expectation value [90].

As a consequence of the nontrivial quark rotation matrices, the λ'_{ijk} coupling in Eq. (1.5) also has to be rotated from the weak basis into the quark mass basis for a comparison with experimental data. In the case of up-type mixing, the $L_i Q_j \bar{D}_k$ interactions of the superpotential (1.1) in the quark mass basis are in terms of SU(2) component superfields

$$\lambda'_{ijk}[N_i D_j^m - E_i (\mathbf{V_{CKM}^+})_{jl} U_l^m] \bar{D}_k^m. \tag{2.16}$$

In the case of down-mixing they are

$$\lambda'_{ijk}[N_i (\mathbf{V}_{\rm CKM})_{jl} D_l^m - E_i U_j^m] (\mathbf{V_{CKM}^+})_{nk} \bar{D}_n^m. \tag{2.17}$$

See also Ref. [59]. However, for slepton production cross sections, we do not take into account these CKM effects. If needed, the corresponding rescaling of the λ' coupling can be done easily. Furthermore, the subdominant interactions, which include nondiagonal matrix elements of $\mathbf{V}_{\rm CKM}$, do not allow for large production cross sections since λ' enters only quadratically.

D. Renormalization group equations

One of the most important consequences of including B_3 effects in SUSY models is that the LSP is no longer stable. This is of special interest for phenomological studies if the LSP couples directly to the dominant B_3 operator. This leads to large LSP decay widths and to distinctive final state signatures.

In the scenarios considered in this work, cf. Eq. (1.5), the dominant coupling is a λ'_{ijk}; for $i \neq 3$ it does not couple to the $\tilde{\tau}_1$ LSP. However, the RGEs of the B_3 couplings are coupled via nondiagonal entries of Higgs-Yukawa matrices, and a λ'_{ijk} generates dynamically other B_3 couplings. Among those, we want to focus on the λ_{i33}, which do couple directly to the $\tilde{\tau}_1$ LSP.

The aim of the next two sections is to study the RGEs of the dominant λ'_{ijk} and to quantitatively determine the generated λ_{i33}. We then use these results to predict the low energy spectrum of B_3 mSUGRA scenarios given by Eq. (1.5). We will also derive approximate formulæ that allow for a numerical implementation of the running of the couplings.

The full renormalization group equations for the B_3 couplings λ'_{ijk} and λ_{i33} are [10,30,31]

$$16\pi^2 \frac{d}{dt}\lambda'_{ijk} = \lambda'_{ijl}\gamma^{D_k}_{D_l} + \lambda'_{ilk}\gamma^{Q_j}_{Q_l} + \lambda'_{ljk}\gamma^{L_i}_{L_l} - (\mathbf{Y}_D)_{jk}\gamma^{L_i}_{H_1}, \tag{2.18}$$

$$16\pi^2 \frac{d}{dt}\lambda_{i33} = \lambda_{i3l}\gamma^{E_3}_{E_l} + \lambda_{il3}\gamma^{L_3}_{L_l} + \lambda_{l33}\gamma^{L_i}_{L_l} - (\mathbf{Y}_E)_{33}\gamma^{L_i}_{H_1} + (\mathbf{Y}_E)_{i3}\gamma^{L_3}_{H_1}, \tag{2.19}$$

with $t = \ln Q$, Q being the renormalization scale. The anomalous dimensions γ are listed in [10] at one-loop level and in [31] at two-loop level. The RGEs simplify considerably under the assumption of the single B_3 coupling dominance hypothesis [60,91]. Products of two or more B_3 couplings including quadratic contributions of the dominant coupling can be neglected for $\lambda' \lesssim \mathcal{O}(10^{-2})$. In this limit, the one-loop anomalous dimensions read

$$\begin{aligned}
\gamma^{Q_i}_{Q_j} &= (\mathbf{Y}_D\mathbf{Y}_D^+)_{ij} + (\mathbf{Y}_U\mathbf{Y}_U^+)_{ij} - \delta^i_j\left(\frac{1}{30}g_1^2 + \frac{3}{2}g_2^2 + \frac{8}{3}g_3^2\right),\\
\gamma^{D_i}_{D_j} &= 2(\mathbf{Y}_D^+\mathbf{Y}_D)_{ji} - \delta^i_j\left(\frac{2}{15}g_1^2 + \frac{8}{3}g_3^2\right),\\
\gamma^{L_i}_{L_j} &= (\mathbf{Y}_E\mathbf{Y}_E^+)_{ij} - \delta^i_j\left(\frac{3}{10}g_1^2 + \frac{3}{2}g_2^2\right),\\
\gamma^{E_i}_{E_j} &= 2(\mathbf{Y}_E^+\mathbf{Y}_E)_{ji} - \delta^i_j\left(\frac{6}{5}g_1^2\right),\\
\gamma^{L_i}_{H_1} &= -3\lambda'_{iaq}(\mathbf{Y}_D)_{aq} - \lambda_{ibq}(\mathbf{Y}_E)_{bq},
\end{aligned} \tag{2.20}$$

where g_1, g_2, g_3 are the three gauge couplings.

From Eqs. (2.19) and (2.20), we see that the terms related to $\gamma^{L_i}_{H_1}$ allow for the dynamical generation of λ_{i33} by a nonzero λ'_{iaq} coupling [and *vice versa* for Eq. (2.18)]. All other terms in Eq. (2.19) only alter the running of λ_{i33} once it is generated. The RGEs can be further simplified. At one-loop level, all B_3 couplings but the dominant λ'_{ijk} and the generated λ_{i33} can be neglected in the RGEs, since they must be generated first by λ' and thus contribute at two-loop level only.

Since we work in a diagonal charged lepton Yukawa basis, the last term in Eq. (2.19), proportional to $(\mathbf{Y}_E)_{i3}$ does not contribute to the running of λ_{i33}. It is only nonzero if $i = 3$, but owing to the ij-antisymmetry of λ_{ijk}, no coupling is generated in this case ($\lambda_{333} = 0$).

Next, a general ordering of the parameters in the anomalous dimensions is [92]

$$g_3^2 > (\mathbf{Y}_U)^2_{33} > g_2^2 > g_1^2 > (\mathbf{Y}_D)^2_{33} > (\mathbf{Y}_E)^2_{33}, \tag{2.21}$$

and all other entries of the $\mathbf{Y}$ matrices are smaller by at least 1 order of magnitude [93]. The contributions to the RGEs are thus largest for diagonal anomalous dimensions.

As a result, the RGEs for a nonzero λ'_{ijk} at the GUT scale and a generated λ_{i33} reduce to

$$\begin{aligned}
16\pi^2 \frac{d}{dt}\lambda'_{ijk} &= \lambda'_{ijk}\Big[-\frac{7}{15}g_1^2 - 3g_2^2 - \frac{16}{3}g_3^2 \\
&\quad + (\mathbf{Y}_D)^2_{33}(2\delta_{k3} + \delta_{j3} + 3\delta_{j3}\delta_{k3}) \\
&\quad + (\mathbf{Y}_U)^2_{33}\delta_{j3} + (\mathbf{Y}_E)^2_{33}\delta_{i3}\Big],
\end{aligned} \tag{2.22}$$

$$\begin{aligned}
16\pi^2 \frac{d}{dt}\lambda_{i33} &= \lambda_{i33}\Big[-\frac{9}{5}g_1^2 - 3g_2^2 + 4(\mathbf{Y}_E)^2_{33}\Big] \\
&\quad + 3\lambda'_{ijk}(\mathbf{Y}_E)_{33}(\mathbf{Y}_D)_{jk}.
\end{aligned} \tag{2.23}$$

A similar analytical approximation for the generation of λ is derived in [51]. But the effect of the gauge couplings is neglected there. See also Ref. [81].

The last term in Eq. (2.23) induces the dynamical generation of λ_{i33}. Diagrammatically, this process can be understood as shown in Fig. 1. We see that at one loop the lepton-doublet superfield mixes with the Higgs doublet superfield H_d via the B_3 coupling λ'_{ijk} and the standard down-quark Yukawa coupling. H_d then couples via the tau Yukawa coupling $(\mathbf{Y}_E)_{33}$ purely leptonically. The resulting effective interaction is of the λ_{i33} type.

It is important to notice that the generation is related to $(\mathbf{Y}_D)_{jk}$. Whether a given λ'_{ijk} can generate λ_{i33} or not depends on whether $(\mathbf{Y}_D)_{jk} \neq 0$. For $j \neq k$ it thus depends crucially on the origin of the CKM mixing: is it dominantly down-type or up-type mixing? In case of down-type mixing, all entries of the $\mathbf{Y}_D$ matrix are nonzero, and all λ'_{ijk} can therefore generate a λ_{i33}. In contrast, if the quark mixing takes place in the up sector, only the diagonal entries of $\mathbf{Y}_D$ are nonzero and $j = k$ is required. The flavor and size of the generated coupling depends on $\tan\beta$ and on the precise j, k configuration. A strong ordering is expected that goes along with the ordering of the entries of the $\mathbf{Y}_D$ matrix.

In order to study the running of the B_3 couplings, the RGEs for the Yukawa matrix elements $(\mathbf{Y}_D)_{jk}$, $(\mathbf{Y}_U)_{33}$, and $(\mathbf{Y}_E)_{33}$ and the gauge couplings are also needed. The full RGEs for the Yukawa couplings are given in [10,30]. Applying the single coupling dominance hypothesis, neglecting quadratic terms in λ'_{ijk}, and considering only the dominant terms in Eq. (2.21), they read

$$\begin{aligned}
16\pi^2 \frac{d}{dt}(\mathbf{Y}_U)_{33} &= (\mathbf{Y}_U)_{33}\Big[-\frac{13}{15}g_1^2 - 3g_2^2 - \frac{16}{3}g_3^2 \\
&\quad + 6(\mathbf{Y}_U)^2_{33} + (\mathbf{Y}_D)^2_{33}\Big],
\end{aligned} \tag{2.24}$$

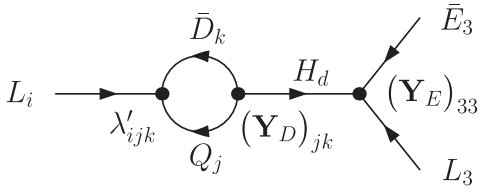

FIG. 1. Superfield diagram for the dynamical generation of λ_{i33} by λ'_{ijk} at one-loop order, see Eq. (2.23).

$$16\pi^2 \frac{d}{dt}(\mathbf{Y}_E)_{33} = (\mathbf{Y}_E)_{33}\Big[-\frac{9}{5}g_1^2 - 3g_2^2 + 4(\mathbf{Y}_E)_{33}^2 + 3(\mathbf{Y}_D)_{33}^2\Big], \quad (2.25)$$

$$16\pi^2 \frac{d}{dt}(\mathbf{Y}_D)_{jk} = (\mathbf{Y}_D)_{jk}\Big[-\frac{7}{15}g_1^2 - 3g_2^2 - \frac{16}{3}g_3^2 + (\mathbf{Y}_D)_{33}^2(3 + \delta_{j3} + 2\delta_{k3}) + (\mathbf{Y}_U)_{33}^2\delta_{j3} + (\mathbf{Y}_E)_{33}^2\Big]. \quad (2.26)$$

The one-loop order RGEs for the three gauge couplings within the MSSM are given by [30]

$$16\pi^2 \frac{d}{dt} g_i = b_i g_i^3, \quad (2.27)$$

with $b_i = \{33/5, 1, -3\}$ for $i = 1, 2, 3$. Thus, in total, a set of nine coupled differential equations, Eqs. (2.22), (2.23), (2.24), (2.25), (2.26), and (2.27), has to be solved [94].

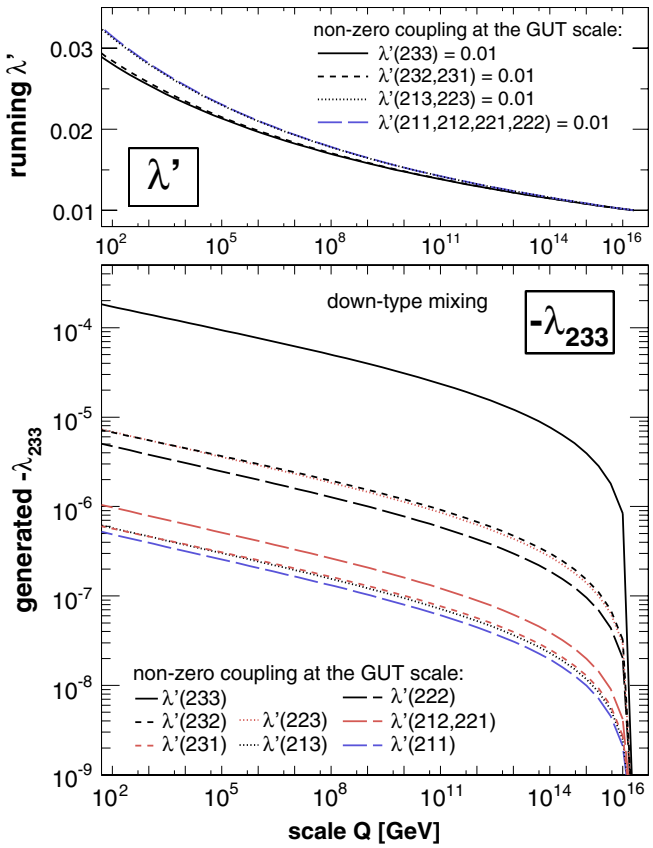

FIG. 2 (color online). Running of B_3 couplings assuming a single nonzero $\lambda' = 0.01$ coupling at the GUT scale (upper panel) leading to a nonzero λ_{233} coupling (lower panel) at lower scales within the B_3 mSUGRA scenario Set A for down-type mixing.

E. Numerical results

For the numerical implementation of the RGEs we start from the framework provided by SOFTSUSY2.0.10[89]. First, SOFTSUSY evaluates all necessary parameters at the SUSY scale

$$Q_{\text{susy}} = \sqrt{m_{\tilde{t}_1}(Q_{\text{susy}})m_{\tilde{t}_2}(Q_{\text{susy}})}. \quad (2.28)$$

In a second step, we apply the (R-parity conserving) RGEs (2.24), (2.25), (2.26), and (2.27) to run the Yukawa couplings and gauge couplings up to the GUT scale. Here, we add the B_3 couplings $\lambda'_{ijk} \neq 0|_{\text{GUT}}$ and $\lambda_{i33} = 0|_{\text{GUT}}$ and evolve these couplings down to the scale Q using the above given B_3 RGEs (2.22) and (2.23). We have implemented the RGEs using a standard Runge Kutta formalism [95].

In Figs. 2 and 3, we show the running of different λ'_{2jk} couplings, starting with $\lambda'_{ijk} = 0.01|_{\text{GUT}}$, for the case of down-type and up-type mixing, respectively. In the corresponding lower panel, we show the scale dependence of the generated $\lambda_{323} = -\lambda_{233}$ coupling. Here, we use the mSUGRA parameters of Set A ($\tan\beta = 13$).

We see that the dominant λ'_{ijk} coupling grows by about a factor of 3, running from the GUT scale to the weak scale. This effect is mainly due to the gauge couplings, see

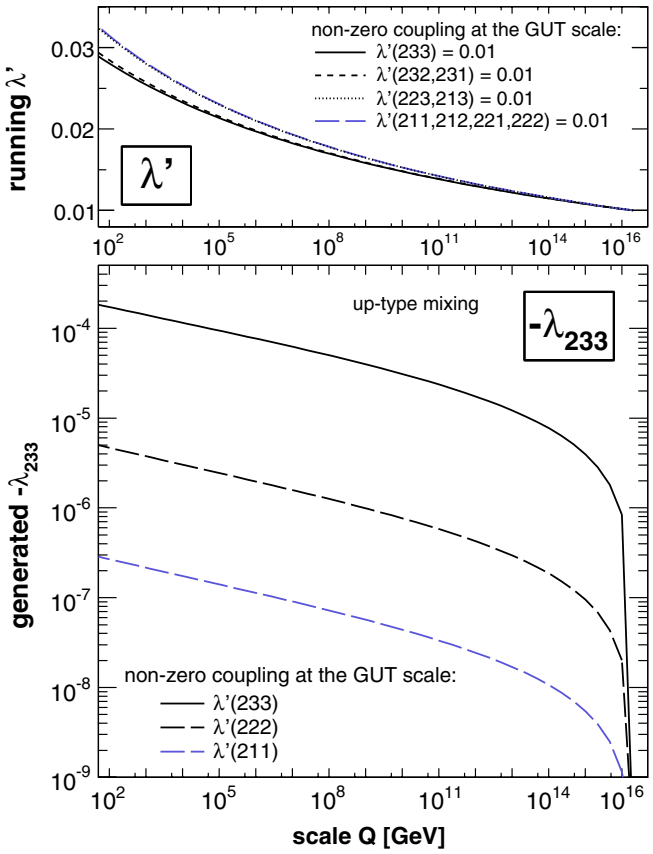

FIG. 3 (color online). Same as Fig. 2, but for quark mixing in the up-sector.

Ref. [81], where the Yukawa couplings were omitted. Including the Yukawa couplings reduces this effect, maximally for $j = k = 3$. The generated λ_{233} coupling is at least 2 orders of magnitude smaller than the original λ' coupling. Furthermore, it depends sensitively on the flavor structure (ijk) of the original λ' coupling. This reflects the dependence on the Yukawa matrix $(\mathbf{Y}_D)_{jk}$. In case of down-type mixing, the ordering of the corresponding entries is

$$(\mathbf{Y}_D)_{33} > (\mathbf{Y}_D)_{23,32} > (\mathbf{Y}_D)_{22} > (\mathbf{Y}_D)_{12,21} > (\mathbf{Y}_D)_{13,31} > (\mathbf{Y}_D)_{11}, \tag{2.29}$$

reflecting precisely the ordering of the generated couplings in Fig. 2. Small differences between the couplings generated by λ'_{i23} (λ'_{i13}) or λ'_{i32} (λ'_{i31}) are related to the different running of the respective λ' and $(\mathbf{Y}_D)_{jk}$ coupling, depending in turn on whether j or k equals 3.

In the case of up-type mixing, Fig. 3, not all λ' couplings can generate a λ. Since the down Yukawa coupling is diagonal, $j = k$ is required. Other couplings can generate λ_{i33} at higher loop levels only and are not included in our approximations.

Our results can easily be translated to other scenarios: The running of the dominant coupling λ' is mainly driven by gauge interactions, Eq. (2.22), and thus depends only weakly on the specific SUSY parameters. The dependence of the generated coupling λ on SUSY parameters is more involved but we expect $\tan\beta$ to have the largest impact. In general, the generated λ coupling scales with $\tan^2\beta$,

$$\lambda_{i33} \propto \tan^2\beta, \tag{2.30}$$

if $\tan^2\beta \gg 1$. This is because the down-quark Yukawa couplings $(\mathbf{Y}_D)_{jk}$ [and the tau Yukawa coupling $(\mathbf{Y}_E)_{33}$] are proportional to $1/\cos\beta = \sqrt{1 + \tan^2\beta}$, which directly follows from Eqs. (2.13), (2.14), and (2.15). Therefore, the magnitude of the generated λ coupling for other scenarios can be estimated by rescaling λ of Fig. 2 and Fig. 3 according to Eq. (2.30).

F. Comparison with the program SOFTSUSY

In this section, we compare our results for λ'_{ijk} and the generated coupling λ_{i33} at the SUSY scale, Eq. (2.28), with an unpublished version of SOFTSUSY [96]. This version of SOFTSUSY contains the complete one-loop RGEs for λ'_{ijk} (2.18) and λ_{i33} (2.19), without our approximations.

We show in Table II our results and the results of SOFTSUSY for the case of down-type mixing and up-type mixing assuming different couplings $\lambda'_{ijk} = 0.01$ at the GUT scale. For the other parameters, we consider the Set A of Eq. (2.7).

At the SUSY scale, the differences between our results and SOFTSUSY for the case of down-type mixing, are less than 2% for all λ'_{ijk} couplings and less than 4% for the λ_{i33}, respectively. In the case of up-type mixing, we find the same for the couplings λ'_{ijk} with $j = k$. However, for $j \neq k$ and up-type mixing, we observe a discrepancy between our results and SOFTSUSY for the coupling λ_{233} generated by $\lambda'_{223} \neq 0|_{\mathrm{GUT}}$ and $\lambda'_{231} \neq 0|_{\mathrm{GUT}}$, respectively. This behavior can easily be understood.

The off-diagonal Yukawa matrix elements $(\mathbf{Y}_D)_{jk}$ are equal to zero at the weak scale for up-type mixing. Running from the weak scale to the GUT scale generates Yukawa couplings $(\mathbf{Y}_D)_{jk}$, $j \neq k$, at the one-loop level [10,30]. The generation of λ_{233} via Eq. (2.23) occurs therefore formally at two-loop level and has been neglected in our approximation. In SOFTSUSY this two-loop effect is taken into account and small couplings are generated also for $j \neq k$ and up-type mixing. Compared to the case of down-type mixing, see Table II, the λ_{233} couplings are suppressed by 5 (with $\lambda'_{231} = 0.01|_{\mathrm{GUT}}$) and 3 (with $\lambda'_{223} = 0.01|_{\mathrm{GUT}}$) orders of magnitude. Note that the generation of $(\mathbf{Y}_D)_{jk}$ is not the only two-loop effect that enters the full RGEs [10,30,31].

Therefore, our approximation for the generation of λ_{i33} by a nonzero λ'_{ijk} at the GUT scale (2.23) breaks down in the case of up-type mixing and $j \neq k$. But concerning $\tilde{\tau}_1$ LSP decays, the corresponding 2-body decay branching ratio for λ_{i33} is negligible compared to the 4-body decay

TABLE II. Comparison between our results, Eqs. (2.22) and (2.23), and the results of an unpublished version of SOFTSUSY [96] for λ'_{ijk} and the generated coupling λ_{i33} at the SUSY scale, Eq. (2.28). We choose different couplings $\lambda'_{ijk} = 0.01$ at the GUT scale as given in the first column of the table. The running of λ'_{ijk} is the same for down- and up-type quark mixing. The generation of λ_{i33} depends on the quark mixing assumptions and the values at the SUSY scale are given separately. The remaining mSUGRA parameters are these of Set A (2.7).

Set A	λ'_{ijk}		λ_{i33} (down-type mixing)		λ_{i33} (up-type mixing)	
	Equation (2.22)	SOFTSUSY	Equation (2.23)	SOFTSUSY	Equation (2.23)	SOFTSUSY
λ'_{211}	2.82×10^{-2}	2.85×10^{-2}	-3.96×10^{-7}	-3.89×10^{-7}	-2.17×10^{-7}	-2.13×10^{-7}
λ'_{231}	2.58×10^{-2}	2.61×10^{-2}	-4.65×10^{-7}	-4.80×10^{-7}	0	$+2.06 \times 10^{-12}$
λ'_{223}	2.81×10^{-2}	2.83×10^{-2}	-5.55×10^{-6}	-5.73×10^{-6}	0	-8.45×10^{-9}
λ'_{233}	2.55×10^{-2}	2.58×10^{-2}	-1.41×10^{-4}	-1.42×10^{-4}	-1.42×10^{-4}	-1.43×10^{-4}
λ'_{311}	2.81×10^{-2}	2.84×10^{-2}	0	0	0	0

branching ratio via λ'_{ijk}, and our approximations are applicable for such phenomenological studies. For example, the 2-body decay branching ratio for up-type mixing and $\lambda'_{231} = 0.01|_{\rm GUT}$ or $\lambda'_{223} = 0.01|_{\rm GUT}$ is less than 10^{-4} in Set A.

We conclude that our approximations are valid for the signal and decay rates that we study in this work. We also note that we have provided an independent check of the yet-to-be published version of SOFTSUSY [96]. Using a different set of mSUGRA parameters leads to a similar level of agreement.

III. $\tilde{\tau}_1$ LSP DECAYS IN B_3 MSUGRA

A. General LSP decay modes

As we showed in Sec. II, a nonvanishing coupling λ'_{ijk} at the GUT scale generates an additional coupling λ_{i33} at the weak scale, which is roughly at least 2 orders of magnitude smaller than λ'_{ijk}, cf. Figs. 2 and 3. In this section, we compare the possible decay modes of the LSP via these two couplings for different B_3 scenarios.

First, let us discuss $\tilde{\chi}_1^0$ LSP scenarios. The leading order decay modes of the $\tilde{\chi}_1^0$ LSP via the dominant λ'_{ijk} and the generated λ_{i33} couplings are all three body decays

$$\tilde{\chi}_1^0 \xrightarrow{\lambda'_{ijk}} \begin{cases} \ell_i^+ \bar{u}_j d_k, \\ \ell_i^- u_j \bar{d}_k, \end{cases} \qquad \tilde{\chi}_1^0 \xrightarrow{\lambda'_{ijk}} \begin{cases} \bar{\nu}_i \bar{d}_j d_k, \\ \nu_i d_j \bar{d}_k, \end{cases} \tag{3.1}$$

and

$$\tilde{\chi}_1^0 \xrightarrow{\lambda_{i33}} \begin{cases} \ell_i^+ \bar{\nu}_\tau \tau^-, \\ \ell_i^- \nu_\tau \tau^+, \end{cases} \qquad \tilde{\chi}_1^0 \xrightarrow{\lambda_{i33}} \begin{cases} \bar{\nu}_i \tau^+ \tau^-, \\ \nu_i \tau^- \tau^+. \end{cases} \tag{3.2}$$

The corresponding partial widths depend quadratically on λ'_{ijk} and λ_{i33}, respectively [97–100]. Therefore, the $\tilde{\chi}_1^0$ decay via λ_{i33} is heavily suppressed and a $\tilde{\chi}_1^0$ LSP decays predominantly via λ'_{ijk} into SM particles.

The situation changes if one considers B_3 mSUGRA scenarios with a $\tilde{\tau}_1$ LSP, where the $\tilde{\tau}_1$ couples not directly to the $L_i Q_j \bar{D}_k$ operator, i.e. $i = 1, 2$. In this case, the $\tilde{\tau}_1$ must first couple to a virtual gaugino. The gaugino then couples to a virtual sfermion, which then decays via λ'_{ijk}, resulting in a 4-body decay of the $\tilde{\tau}_1$ LSP. The possible decay modes via a virtual neutralino are

$$\tilde{\tau}_1^- \xrightarrow{\lambda'_{ijk}} \begin{cases} \tau^- \ell_i^+ \bar{u}_j d_k, \\ \tau^- \ell_i^- u_j \bar{d}_k, \\ \tau^- \bar{\nu}_i \bar{d}_j d_k, \\ \tau^- \nu_i d_j \bar{d}_k. \end{cases} \tag{3.3}$$

Four-body decays via a virtual chargino are also possible, but they are suppressed due to the higher chargino mass in comparison to the lightest neutralino mass $m(\tilde{\chi}_1^\pm) > m(\tilde{\chi}_1^0)$. Furthermore, the (mainly right-handed) $\tilde{\tau}_1$ LSP couples stronger to the (binolike) lightest neutralino than to the (winolike) lightest chargino.

On the other hand, the $\tilde{\tau}_1$ can directly decay via λ_{i33} into only two SM particles

$$\tilde{\tau}_1^- \xrightarrow{\lambda_{i33}} \begin{cases} \tau^- \bar{\nu}_i, \\ \tau^- \nu_i, \\ \ell_i^- \nu_\tau. \end{cases} \tag{3.4}$$

We show in Fig. 4 (Fig. 5), example diagrams for the 4-body (2-body) decay of a $\tilde{\tau}_1$ LSP via λ'_{2jk} (λ_{233}). Although the 2-body decay suffers from the small coupling, the 4-body decay is phase-space suppressed as well as by heavy propagators. Which decay mode dominates depends strongly on the parameters at the GUT scale. We will discuss in detail this topic in the next section.

As a third type of B_3 mSUGRA scenarios we want to mention $\tilde{\tau}_1$ LSP scenarios with a dominant λ'_{3jk} coupling. Here, the dominant B_3 operator couples directly to the $\tilde{\tau}_1$ LSP and allows for a 2-body decay of the $\tilde{\tau}_1$ into two jets,

$$\tilde{\tau}_1^- \xrightarrow{\lambda'_{3jk}} \bar{u}_j d_k. \tag{3.5}$$

λ'_{3jk} cannot generate λ_{333} via the RGEs, because λ_{ijk} has to be antisymmetric in the indices i, j. λ_{3nn} with $n \neq 3$ will be generated by the muon ($n = 2$) or electron ($n = 1$) Higgs-Yukawa coupling, cf. Eq. (2.23). But since these Yukawa couplings are so small, the decay via λ_{3nn} is too small to be seen.

For $j = 3$, the up-type quark in Eq. (3.5) is a top quark and hence the decay Eq. (3.5) is kinematically forbidden for $m_{\tilde{\tau}_1} < m_t$. The $\tilde{\tau}_1$ LSP then decays in a 3-body decay

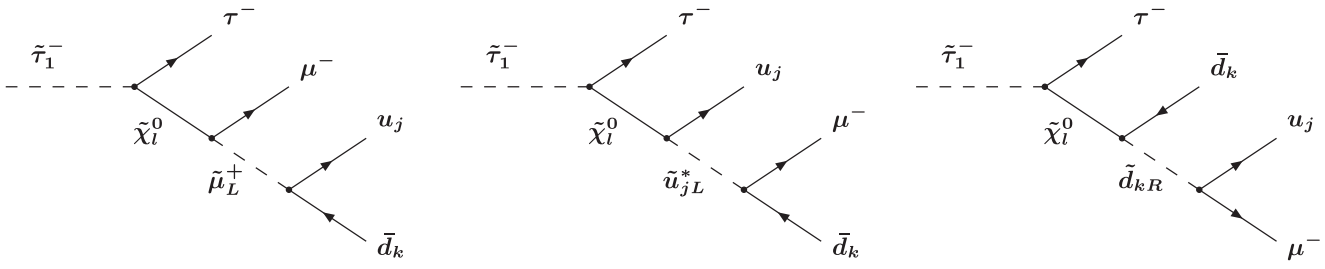

FIG. 4. Feynman diagrams contributing to the 4-body decay $\tilde{\tau}_1^- \to \tau^- \mu^- u_j \bar{d}_k$ of the $\tilde{\tau}_1$ LSP via λ'_{2jk}. In this example the $\tilde{\tau}_1$ decays via a virtual neutralino $\tilde{\chi}_l^0$ ($l = 1, 2, 3, 4$) into a tau τ^-, a muon μ^-, an up-type quark u_j of generation j and a down-type antiquark $\bar{d}_k$ of generation k.

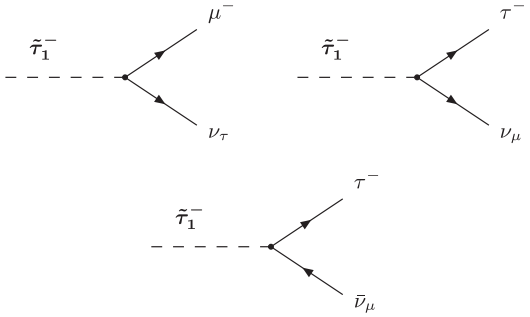

FIG. 5. Feynman diagrams leading to the 2-body decays of the $\tilde{\tau}_1$ LSP via the generated coupling λ_{233}. The $\tilde{\tau}_1$ decays either into a muon μ^- and a neutrino or into a τ^- and a neutrino.

mode via a virtual top quark into a W boson and two jets, where at least one jet is a b jet

$$\tilde{\tau}_1^- \xrightarrow{\lambda'_{33k}} W^- \bar{b} d_k. \tag{3.6}$$

We present the squared matrix element and the partial width of this process in Appendix B, which to our knowledge has not been given in the literature so far.

B. Dependence of $\tilde{\tau}_1$ decays on mSUGRA parameters

In this section, we investigate the conditions at the GUT scale that lead to 2-body decays of the $\tilde{\tau}_1$ LSP. We assume a nonvanishing λ'_{2jk} coupling at the GUT scale. This can easily be generalized to λ'_{1jk}. We point out that the branching ratios of the $\tilde{\tau}_1$ LSP do not depend on the magnitude of λ'_{ijk}, since they cancel in the ratio. The following discussion is therefore also applicable to scenarios where the couplings are too small to produce a significant number of single slepton events at the LHC but where the $\tilde{\tau}_1$ LSP is produced in cascade decays of pair produced SUSY particles.

For the numerical implementation we use SOFTSUSY2.0.10 [89] to calculate the mass spectrum at the SUSY scale, Eq. (2.28). In addition, we use our own program to calculate λ'_{ijk} and λ_{i33} at the SUSY scale as described in Sec. II E. We then pipe the mass spectrum and the couplings through ISAWIG1.200, which is linked to ISAJET7.75 [101]. ISAJET calculates the 2-body partial width of the SUSY particles and produces an output for HERWIG [102–104]. We use a special version of HERWIG6.510, which also calculates the 4-body decays of the $\tilde{\tau}_1$ LSP [105]. As an output, we consider the total 2-body decay branching ratio of the $\tilde{\tau}_1$ LSP, BR_2. It is defined as

$$\mathrm{BR}_2 = \frac{1}{1 + \Gamma_4/\Gamma_2}, \tag{3.7}$$

where Γ_2 and Γ_4 denote the sums of the partial widths for the 2- and 4-body decays, respectively.

We first show in Fig. 6 (Fig. 7) the $\tan\beta$ dependence of the 2-body decay branching ratio. We give values for different nonvanishing couplings λ'_{2jk} at the GUT scale, and we assume quark mixing in the down (up) sector.

Nearly all $\tilde{\tau}_1$ LSPs will decay via a 2-body decay for large values of $\tan\beta$, i.e. $\tan\beta \gtrsim 30$, and down-type mixing. In the case of up-type mixing this is also true for λ'_{211}, λ'_{222} and λ'_{233}. This behavior can be easily explained with the help of Eq. (3.7). The partial widths Γ_2, Γ_4 can be approximated by [10]

$$\Gamma_2 \propto \lambda^2_{233} m_{\tilde{\tau}_1}, \tag{3.8}$$

$$\Gamma_4 \propto \lambda'^2_{2jk} \frac{m^7_{\tilde{\tau}_1}}{m^2_{\tilde{\chi}} m^4_{\tilde{f}}}. \tag{3.9}$$

$m_{\tilde{\chi}}$ denotes the mass of the relevant gaugino and $m_{\tilde{f}}$ denotes the mass of the virtual sfermion, which couples directly to $L_2 Q_j \bar{D}_k$, cf. Fig. 4.

As we argued in Sec. II E, the generated coupling λ_{233} scales roughly with $\tan^2\beta$, cf. Eq. (2.30). Therefore, Γ_2 scales with $\tan^4\beta$. At the same time, λ'_{211} is hardly affected by $\tan\beta$. This is the main effect that enhances BR_2 for large $\tan\beta$.

Furthermore, increasing $\tan\beta$ increases the contribution from the tau Yukawa couplings to the various RGEs. This is encoded in the function X_τ, Eq. (2.4), which is proportional to $(1 + \tan^2\beta)$. As can be seen in Eq. (2.4), increasing $\tan\beta$ and X_τ reduces the mass of the right- and left-handed stau and therefore, with Eq. (2.5), the mass of the

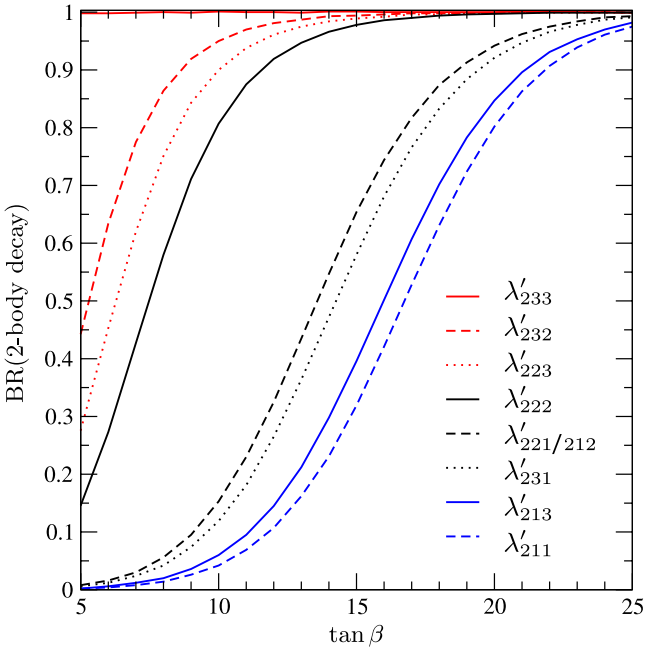

FIG. 6 (color online). 2-body decay branching ratio as a function of $\tan\beta$ for different dominating λ'_{2jk} couplings at the GUT scale. The quark mixing is in the down sector, and the mSUGRA parameters are $M_0 = 0$ GeV, $M_{1/2} = 500$ GeV, $A_0 = 600$ GeV, $\mathrm{sgn}(\mu) = +1$.

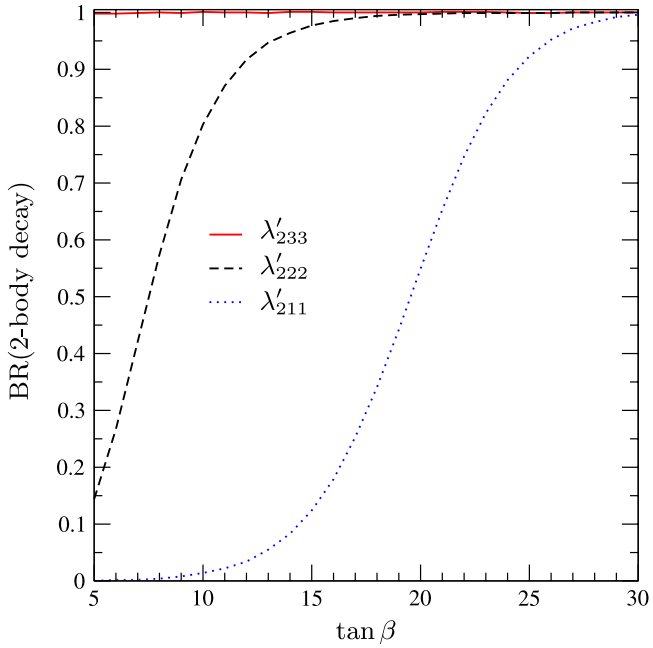

FIG. 7 (color online). 2-body decay branching ratio as a function of $\tan\beta$ for different dominating λ'_{2jk} couplings at the GUT scale. The quark mixing is in the up sector, and the mSUGRA parameters are $M_0 = 0$ GeV, $M_{1/2} = 500$ GeV, $A_0 = 600$ GeV, $\mathrm{sgn}(\mu) = +1$. Couplings λ'_{2jk} for which the 2-body decay branching ratio nearly vanishes are not shown.

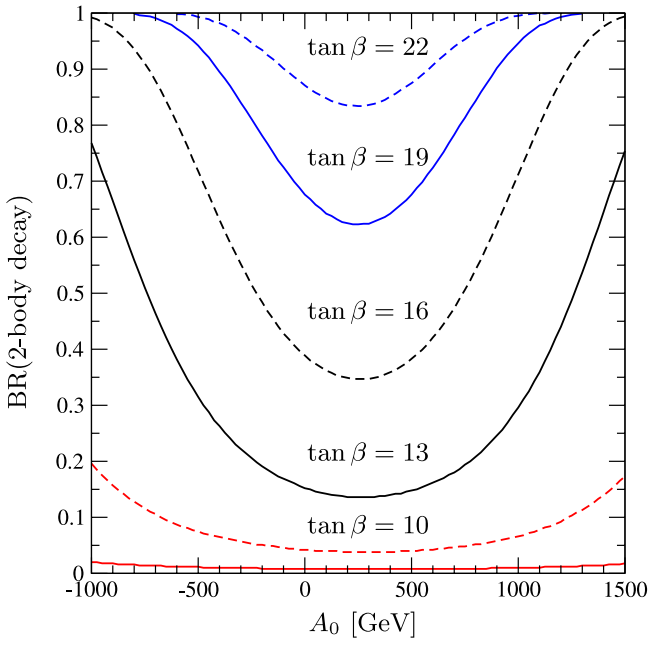

FIG. 8 (color online). 2-body decay branching ratio as a function of A_0 for nonvanishing λ'_{211} at the GUT scale and different $\tan\beta$. We assume down-type quark mixing. The other mSUGRA parameters are $M_0 = 0$ GeV, $M_{1/2} = 500$ GeV, $\mathrm{sgn}(\mu) = +1$. The solid red curve (bottom) corresponds to $\tan\beta = 7$.

$\tilde{\tau}_1$ LSP, $m_{\tilde{\tau}_1}$. Furthermore, the off-diagonal matrix elements of the stau mass matrix Eq. (2.2) also increase with $\tan\beta$. This leads to a stronger mixing between the right- and left-handed stau and lowers the mass of the $\tilde{\tau}_1$, cf. Eq. (2.5).

Note that Γ_4/Γ_2 is proportional to $m^6_{\tilde{\tau}_1}$. According to Eq. (3.7), the 2-body decay branching ratio therefore strongly increases for decreasing $m_{\tilde{\tau}_1}$.

We observe in Fig. 6 also a large hierarchy between the different couplings λ'_{2jk}. For example, a dominant λ'_{233} coupling leads to $\mathrm{BR}_2 \approx 100\%$ for any value of $\tan\beta$, whereas for λ'_{211} this is only the case for $\tan\beta \gtrsim 25$. This hierarchy reflects the hierarchy of the down-quark Yukawa matrix elements, Eq. (2.29), which enter as the dominant term in the RGE of λ_{233}, Eq. (2.23).

For up-type quark mixing, Fig. 7, and $j \neq k$ the down-quark Yukawa matrix elements and therefore BR_2 are nearly vanishing.

We investigate the dependence of BR_2 on A_0 in Fig. 8, for a dominant coupling λ'_{211} and down-type mixing. We see a minimum at $A_0 \approx 250$ GeV. Here, BR_2 is reduced by up to 70% compared to $A_0 = \pm 1$ TeV. The minimum and the position of the minimum is dominated by the following two effects.

The right-handed stau couples to a left-handed stau (tau sneutrino) and a neutral Higgs (charged Higgs) via a trilinear scalar interaction $(\mathbf{h}_E)_{33}$ [10]. The coupling $(\mathbf{h}_E)_{33}$ has dimension one, and in mSUGRA models it is equal to $A_0 \times (\mathbf{Y}_E)_{33}$ at the GUT scale. The RGE of the right-handed scalar tau mass, $m_{\tilde{\tau}_R}$, depends in the following way on $(\mathbf{h}_E)^2_{33}$ [10]

$$\frac{dm_{\tilde{\tau}^2_R}}{dt} = +4(\mathbf{h}_E)^2_{33} + \ldots. \tag{3.10}$$

This term decreases $m_{\tilde{\tau}_R}$ when we go from the GUT scale to the SUSY scale (2.28) due to the plus sign. The (negative) contribution of this term to $m^2_{\tilde{\tau}_R}$ is proportional to the integral of $(\mathbf{h}_E)^2_{33}$ from $t_{\min} = \ln(M_{\mathrm{GUT}})$ to $t_{\max} = \ln(M_Z)$. For the mSUGRA parameters given in Fig. 8, $M_0 = 0$ GeV, $M_{1/2} = 500$ GeV, $\mathrm{sgn}(\mu) = +1$, the integral of $(\mathbf{h}_E)^2_{33}$ is minimal at $A_0 \approx 180$ GeV and, therefore, $m_{\tilde{\tau}_R}$ is maximal. For $m_{\tilde{\tau}_1} = m_{\tilde{\tau}_R}$ this also leads to a maximum of $\Gamma_4/\Gamma_2 \sim m^6_{\tilde{\tau}_1}$ and hence to a minimum of BR_2.

But the lightest stau is an admixture of the right- and left-handed stau. The off-diagonal mass matrix elements B_{LR}, Eq. (2.2), depend also on the value of $(\mathbf{h}_E)_{33}$ at the SUSY scale, Eq. (2.28), through $A_\tau = (\mathbf{h}_E)_{33}/(\mathbf{Y}_E)_{33}$. For $A_0 = 180$ GeV we find $A_\tau \approx -110$ GeV. A negative value of A_τ enhances the effect of L–R mixing, which decreases $m_{\tilde{\tau}_1}$. Therefore, the maximum of $m_{\tilde{\tau}_1}$ as a function of A_0 is shifted to $A_0 \approx 250$ GeV compared to $m_{\tilde{\tau}_R}$. Note however that the A_τ dependence of stau L–R mixing is subdominant around the minimum because of $\mu \tan\beta \gg A_\tau$.

Next, we study the dependence of BR_2 on the universal gaugino mass $M_{1/2}$. We show this behavior in Fig. 9, again for a dominant λ'_{211} and down-type mixing. The 2-body decay branching ratios approach a constant value for increasing $M_{1/2}$. Both, the squared mass of the gauginos, cf. Eq. (2.6), and the squared masses of the sfermions, cf. Eq. (2.1), depend linearly on $M^2_{1/2}$. Therefore,

$$\lim_{M_{1/2}\to\infty} \Gamma_4/\Gamma_2 \propto \frac{m^6_{\tilde{\tau}_1}}{m^2_{\tilde{\chi}} m^4_{\tilde{f}}} = \text{constant}. \tag{3.11}$$

The dependence of BR_2 on $M_{1/2}$ for $M_{1/2} \lesssim 1$ TeV is more involved, because the ratio Γ_4/Γ_2 depends also on the other mSUGRA parameters, mainly through the running sfermion masses, cf. Eq. (2.1). For example, we observe in Fig. 9 that the slope of BR_2 for $M_{1/2} \lesssim 1$ TeV strongly depends on $\tan\beta$. For $\tan\beta = 10$, the slope is small and positive whereas for $\tan\beta \gtrsim 13$ the slope is negative. The magnitude of the slope also increases when we consider larger values of $\tan\beta$. This behavior is again related to the tau Yukawa coupling $(\mathbf{Y}_E)_{33}$ and its effects on the $\tilde{\tau}_1$ mass described by the function X_τ, Eq. (2.4). For large values of $M_{1/2}$, the influence of X_τ on the $\tilde{\tau}_1$ mass nearly vanishes. But as we go to smaller values of $M_{1/2}$ the (negative) contributions due to $(\mathbf{Y}_E)_{33}$ become more and more important. For example, for $\tan\beta = 22$ and $M_{1/2} = 1$ TeV ($M_{1/2} = 400$ GeV) the X_τ term reduces the mass of the right-handed stau by 3% (10%) compared to vanishing

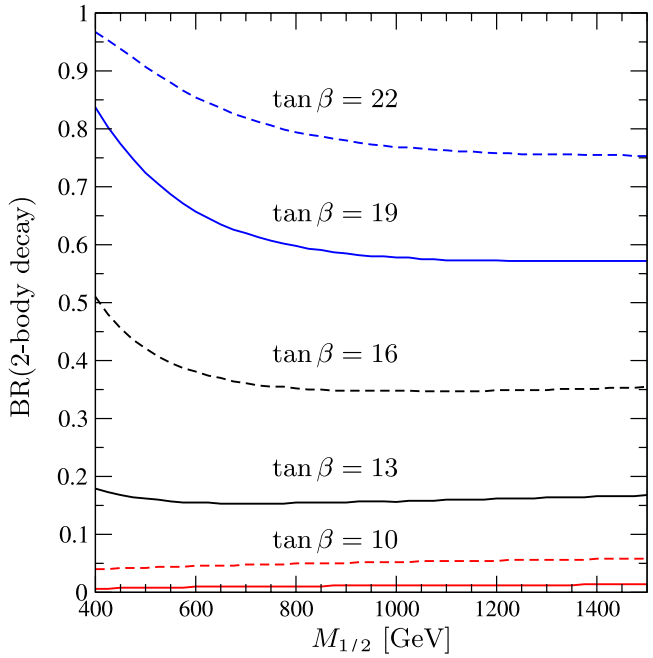

FIG. 9 (color online). 2-body decay branching ratio as a function of $M_{1/2}$ for nonvanishing λ'_{211} at the GUT scale and different $\tan\beta$. We assume quark mixing in the down sector. The other mSUGRA parameters are $M_0 = 0$ GeV, $A_0 = 600$ GeV, $\mathrm{sgn}(\mu) = +1$. The solid red curve (bottom) corresponds to $\tan\beta = 7$.

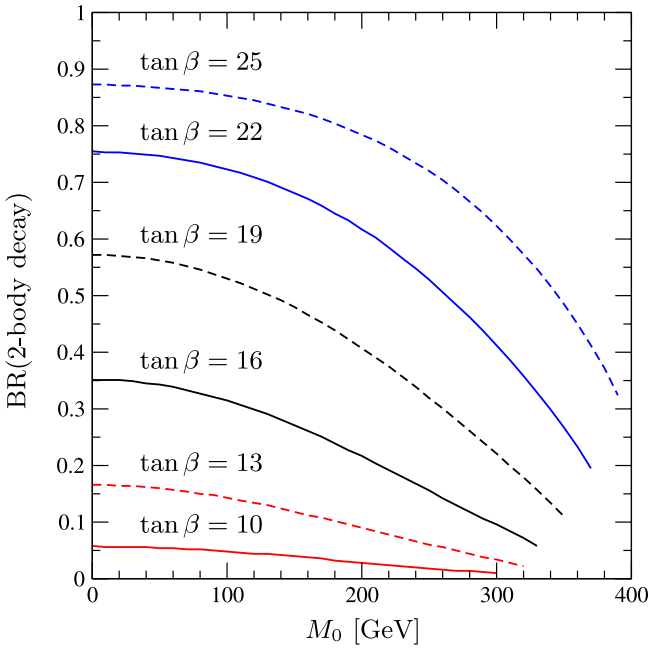

FIG. 10 (color online). 2-body decay branching ratio as a function of M_0 for nonvanishing λ'_{211} at the GUT scale and different $\tan\beta$. We assume quark mixing in the down-sector. The other mSUGRA parameters are $M_{1/2} = 1400$ GeV, $A_0 = 600$ GeV, $\mathrm{sgn}(\mu) = +1$.

$(\mathbf{Y}_E)_{33}$. This reduction of $m_{\tilde{\tau}_1}$ will also reduce Γ_4/Γ_2 resulting in an increase of BR_2. This effect is more pronounced for large $\tan\beta$ because X_τ is proportional to $(1 + \tan^2\beta)$. If we neglect the effect of $(\mathbf{Y}_E)_{33}$, the BR_2 curves in Fig. 9 all get a small positive slope.

Finally, we show in Fig. 10 the dependence of BR_2 on the universal softbreaking scalar mass M_0. Here, we have chosen a rather large value of $M_{1/2}$, $M_{1/2} = 1400$ GeV, because otherwise a $\tilde{\tau}_1$ LSP would exist only in a small interval of M_0.

The behavior of BR_2 can easily be understood. Increasing M_0 increases the mass of the sfermions, Eq. (2.1), but not the mass of the gauginos. Therefore, the nominator of $\Gamma_4/\Gamma_2 \propto m^6_{\tilde{\tau}_1}/(m^2_{\tilde{\chi}} m^4_{\tilde{f}})$ is a polynomial of order $\mathcal{O}(M_0^6)$, whereas the denominator is only a polynomial of order $\mathcal{O}(M_0^4)$. Therefore, the 2-body decay branching ratios fall off for increasing M_0 as shown in Fig. 10. The lines in the figure terminate at values of M_0 above which the $\tilde{\tau}_1$ is no longer the LSP.

IV. RESONANT SINGLE SLEPTON PRODUCTION IN $\tilde{\tau}_1$ LSP SCENARIOS

We now apply the previous discussion to resonant single slepton production in B_3 mSUGRA scenarios with a $\tilde{\tau}_1$ LSP. Charged sleptons $\tilde{\ell}_{Li}$ and sneutrinos $\tilde{\nu}_i$ can be produced singly on resonance at the LHC via $q_k\bar{q}_j$ annihilation processes. The production cross section is proportional to

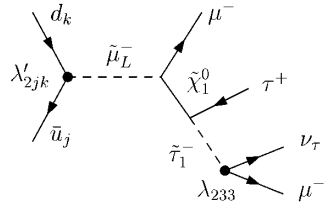

FIG. 11. Example Feynman graph for single slepton production in $\tilde{\tau}_1$ LSP scenarios where the slepton decay proceeds via the generated λ_{233} coupling (2-body decay mode).

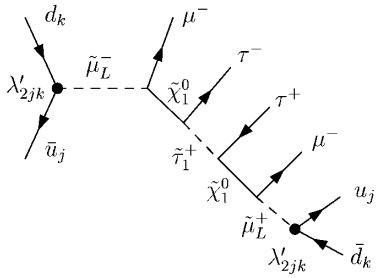

FIG. 12. Example Feynman graph for single slepton production in $\tilde{\tau}_1$ LSP scenarios, where the slepton decay proceeds via the dominant λ'_{2jk} coupling (4-body decay mode).

$|\lambda'_{ijk}|^2$ and therefore large slepton production rates are expected in scenarios with a dominant λ'_{ijk} coupling. The RGE generation of λ_{i33} is important for the subsequent slepton decay in $\tilde{\tau}_1$ LSP scenarios. As discussed in the previous section, a nonvanishing λ_{i33} introduces new 2-body decay channels for the $\tilde{\tau}_1$ LSP. The interplay of these 2-body decays and the 4-body decays via λ'_{ijk} determines the final state signatures. In Figs. 11 and 12, example Feynman graphs for single slepton production, and the subsequent decay in $\tilde{\tau}_1$ LSP scenarios are shown.

It is the aim of this section to first give a general overview of the possible final states for these reactions and second to discuss the special cases $\lambda'_{2jk} \neq 0|_{\mathrm{GUT}}$ and $\lambda'_{3jk} \neq 0|_{\mathrm{GUT}}$ in more detail (Secs. IV B and IV C).

A. General signatures

In the last section, the ratio of 2- to 4-body $\tilde{\tau}_1$ LSP decay rates and its dependence on various SUSY parameters has been studied. Now, we focus on single slepton production in $\tilde{\tau}_1$ LSP scenarios and are interested in the general decay patterns, independent of the precise SUSY parameters. We first give an overview over all possible final states and signatures that could be used as the starting point for an experimental analysis.

A (left-handed) charged slepton or sneutrino can be produced directly via λ'_{ijk} and has several decay modes

$$\bar{u}_j d_k \to \tilde{\ell}_{Li}^- \to \begin{cases} \bar{u}_j d_k, \\ \ell_i^- \tilde{\chi}_m^0, \\ \nu_i \tilde{\chi}_n^-, \end{cases} \tag{4.1}$$

$$\bar{d}_j d_k \to \tilde{\nu}_i \to \begin{cases} \bar{d}_j d_k, \\ \nu_i \tilde{\chi}_m^0, \\ \ell_i^- \tilde{\chi}_n^+. \end{cases} \tag{4.2}$$

Both can decay via the B_3 coupling, which is the inverse production process. It is however suppressed by $|\lambda'_{ijk}|^2$. If $\lambda'_{ijk} \leq \mathcal{O}(10^{-2})$, it contributes typically at the percent level. The dominant decay channels are 2-body decays into a lepton-gaugino pair. Further 3- and more-body decays are expected to be negligible, due to phase-space suppression.

In the case of $j = 3$, the hadronic production of a charged slepton cannot proceed via two quarks as given in Eq. (4.1), due to the vanishing top-quark parton density inside a proton. Instead, the slepton can, for example, be produced via a $g\bar{d}_k$ initiated Compton process in association with a single top quark. Furthermore, the decay into $t\bar{d}_k$ may be kinematically forbidden. In this case, the slepton decays via a virtual top. The corresponding decay width is given in Appendix B. Sneutrino production for $j = 3$ is possible, Eq. (4.2), but due to the low bottom-quark density small cross sections are expected. We do not consider $j = 3$ any further here and refer the reader to [50,69–71] for a detailed investigation of this topic.

For the following discussion, we assume that the produced slepton predominantly decays into a lepton and the lightest neutralino. This assumption is motivated by the fact that we consider $\tilde{\tau}_1$ LSP scenarios. In these scenarios, sleptons are light compared to gauginos and decays into heavier neutralinos or charginos will be kinematically excluded or strongly suppressed. See also the computed branching ratios in explicit SUSY models in [9].

The produced $\tilde{\chi}_1^0$ is not the lightest SUSY particle and will decay further into the $\tilde{\tau}_1$ LSP,

$$\tilde{\chi}_1^0 \to \tau^\mp \tilde{\tau}_1^\pm. \tag{4.3}$$

Since the neutralino is a Majorana fermion, both charge conjugated decays are possible. In most $\tilde{\tau}_1$ LSP scenarios this is the only possible decay mode of the neutralino. However, in some scenarios, the right-handed sleptons $\tilde{\mu}_R$ and $\tilde{e}_R$ are lighter than the $\tilde{\chi}_1^0$ and the additional channels $\tilde{\chi}_1^0 \to \tilde{\ell}_R^\pm \ell^\mp$ are open (for $\ell = \mu, e$). The $\tilde{\ell}_R$ subsequently decays into the $\tilde{\tau}_1$ LSP, a τ, and a lepton via a virtual neutralino

$$\tilde{\chi}_1^0 \to \ell^\mp \tilde{\ell}_R^\pm, \ \tilde{\ell}_R^\pm \to \begin{cases} \ell^\pm \tau^\mp \tilde{\tau}_1^\pm, \\ \ell^\pm \tau^\pm \tilde{\tau}_1^\mp. \end{cases} \tag{4.4}$$

These decay chains have smaller branching ratios (BRs) than the decays in Eq. (4.3). However, they lead to an additional lepton pair in the final state and could be, therefore, of special interest for experimental analyses.

B. $\lambda'_{2jk} \neq 0|_{\mathrm{GUT}}$, $\lambda_{233} \ll \lambda'_{2jk}$

Let us now study more detailed the final state signatures in a scenario with $\lambda'_{2jk} \neq 0|_{\mathrm{GUT}}$ and a generated λ_{233}

coupling, which is small but nonzero at lower scales. In these scenarios, resonant single $\tilde{\mu}_L$ production and resonant single $\tilde{\nu}_\mu$ production at hadron colliders is possible,

$$\begin{aligned} \bar{u}_j d_k &\to \tilde{\mu}_L^- \to \bar{u}_j d_k / \mu^- \tilde{\chi}_1^0, \\ \bar{d}_j d_k &\to \tilde{\nu}_\mu \to \bar{d}_j d_k / \nu_\mu \tilde{\chi}_1^0. \end{aligned} \tag{4.5}$$

As explained above, a small fraction of the sleptons decay via the inverse production process. Predominantly they decay into a lepton and the lightest neutralino, $\tilde{\chi}_1^0$. The decays involving heavier neutralinos or charginos are typically not accessible.

The difference between $\tilde{\mu}_L$ and $\tilde{\nu}_\mu$ production concerns the flavor of the initial quarks involved (which is related to different parton density functions and is thus important for the hadronic cross sections), and the nature of the lepton resulting from the slepton decay. In both processes a neutralino is produced in the predominant decay, which in turn decays into the $\tilde{\tau}_1$ LSP, as given in Eq. (4.3) and (4.4). Finally, the $\tilde{\tau}_1$ decays either via the dominant λ'_{2jk} coupling (4-body decay) or via the generated λ_{233} coupling (2-body decay). For the 4-body decays, only the decays via virtual neutralinos have to be considered. Decay modes via virtual charginos are suppressed due to the larger mass and their weaker couplings to the predominantly right-handed $\tilde{\tau}_1$ LSP. The complete cascade decay chains are listed in Table III.

A classification of all possible final state signatures is given in Table IV, for $\tilde{\mu}_L$ and for $\tilde{\nu}_\mu$ production. For completeness, we include here the direct B_3 decays via λ'_{2jk}, which usually contribute at the percent level for couplings at the order of $\mathcal{O}(10^{-2})$. Neutrinos do not give a signal in a detector and are denoted as missing transverse energy, $\not{E}_T$. Final state quarks are treated as indistinguishable jets j.

The 4-body decays via λ'_{2jk} and the 2-body decays via the inverse production process lead to two jets in the final state. In contrast, the 2-body decays via λ_{233} are purely leptonic. Many cascade decay chains provide missing transverse energy. Furthermore, since we are considering $\tilde{\tau}_1$ LSP scenarios, there is always at least one τ among the final state particles. The experimentally most promising signatures are most likely those involving a large number

TABLE III. Slepton decay chains with all possible final states for single $\tilde{\mu}_L^-$ and single $\tilde{\nu}_\mu$ production via λ'_{2jk}, respectively. The charge conjugated processes are not shown explicitly. Slepton decays into heavier neutralinos or charginos are neglected. The $\tilde{\chi}_1^0$ decays predominantly into a $\tilde{\tau}_1$ LSP and a τ. In some scenarios, decays as in Eq. (4.4) are possible, they are cited in brackets. Owing to the Majorana-type nature of the neutralino two charge conjugated decays of the neutralino are possible (second and third column). In the first column the B_3 coupling involved in the subsequent 4- or 2-body $\tilde{\tau}_1$ decays are given.

	$\bar{u}_j d_k \xrightarrow{\lambda'} \tilde{\mu}_L^- \to \bar{u}_j d_k / \mu^- \tilde{\chi}_1^0$ or $\bar{d}_j d_k \xrightarrow{\lambda'} \tilde{\nu}_\mu \to \bar{d}_j d_k / \nu_\mu \tilde{\chi}_1^0$	
	$\tilde{\chi}_1^0 \to \tau^+ \tilde{\tau}_1^-$ $[\tilde{\chi}_1^0 \to \tau^+ \tilde{\tau}_1^- \ell^+ \ell^-]$	$\tilde{\chi}_1^0 \to \tau^- \tilde{\tau}_1^+$ $[\tilde{\chi}_1^0 \to \tau^- \tilde{\tau}_1^+ \ell^- \ell^+]$
λ'_{2jk}	$\tilde{\tau}_1^- \to \tau^- \mu^- u_j \bar{d}_k$	$\tilde{\tau}_1^+ \to \tau^+ \mu^+ \bar{u}_j d_k$
	$\tilde{\tau}_1^- \to \tau^- \mu^+ \bar{u}_j d_k$	$\tilde{\tau}_1^+ \to \tau^+ \mu^- u_j \bar{d}_k$
	$\tilde{\tau}_1^- \to \tau^- \nu_\mu d_j \bar{d}_k$	$\tilde{\tau}_1^+ \to \tau^+ \bar{\nu}_\mu \bar{d}_j d_k$
	$\tilde{\tau}_1^- \to \tau^- \bar{\nu}_\mu \bar{d}_j d_k$	$\tilde{\tau}_1^+ \to \tau^+ \nu_\mu d_j \bar{d}_k$
λ_{233}	$\tilde{\tau}_1^- \to \tau^- \nu_\mu$	$\tilde{\tau}_1^+ \to \tau^+ \bar{\nu}_\mu$
	$\tilde{\tau}_1^- \to \tau^- \bar{\nu}_\mu$	$\tilde{\tau}_1^+ \to \tau^+ \nu_\mu$
	$\tilde{\tau}_1^- \to \mu^- \nu_\tau$	$\tilde{\tau}_1^+ \to \mu^+ \bar{\nu}_\tau$

TABLE IV. Summary of all possible final states for single slepton production via λ'_{2jk}. Decays involving the dominant λ'_{2jk} coupling and involving the generated λ_{233} coupling are listed separately, cf. Table III. If kinematically allowed, the $\tilde{\chi}_1^0$ may also decay into a light-flavor lepton-slepton pair, which gives rise to an additional $\mu^+\mu^-$ or e^+e^- pair in the final state. The corresponding signatures are given in brackets. The decay via the inverse production process is also listed.

		$\tilde{\mu}_L^-$ production			
λ'_{2jk}	$\tau^+\tau^-$	$\mu^-\mu^\pm$			jj
	$\tau^+\tau^-$	μ^-		$\not{E}_T$	jj
	$[\tau^+\tau^-$	$\mu^-\mu^-\mu^\pm\mu^+$			$jj]$
	$[\tau^+\tau^-$	$\mu^-\mu^-\mu^+$		$\not{E}_T$	$jj]$
	$[\tau^+\tau^-$	$\mu^-\mu^\pm$	e^+e^-		$jj]$
	$[\tau^+\tau^-$	μ^-	e^+e^-	$\not{E}_T$	$jj]$
λ_{233}	$\tau^\pm$	$\mu^-\mu^\mp$		$\not{E}_T$	
	$\tau^+\tau^-$	μ^-		$\not{E}_T$	
	$[\tau^\pm$	$\mu^-\mu^-\mu^\mp\mu^+$		$\not{E}_T$	$]$
	$[\tau^+\tau^-$	$\mu^-\mu^-\mu^+$		$\not{E}_T$	$]$
	$[\tau^\pm$	$\mu^-\mu^\mp$	e^+e^-	$\not{E}_T$	$]$
	$[\tau^+\tau^-$	μ^-	e^+e^-	$\not{E}_T$	$]$
Inv. prod.					jj
		$\tilde{\nu}_\mu$ production			
λ'_{2jk}	$\tau^+\tau^-$	$\mu^\pm$		$\not{E}_T$	jj
	$\tau^+\tau^-$			$\not{E}_T$	jj
	$[\tau^+\tau^-$	$\mu^-\mu^\pm\mu^+$		$\not{E}_T$	$jj]$
	$[\tau^+\tau^-$	$\mu^-\mu^+$		$\not{E}_T$	$jj]$
	$[\tau^+\tau^-$	$\mu^\pm$	e^+e^-	$\not{E}_T$	$jj]$
	$[\tau^+\tau^-$		e^+e^-	$\not{E}_T$	$jj]$
λ_{233}	$\tau^\pm$	$\mu^\mp$		$\not{E}_T$	
	$\tau^+\tau^-$			$\not{E}_T$	
	$[\tau^\pm$	$\mu^-\mu^\mp\mu^+$		$\not{E}_T$	$]$
	$[\tau^+\tau^-$	$\mu^-\mu^+$		$\not{E}_T$	$]$
	$[\tau^\pm$	$\mu^\mp$	e^+e^-	$\not{E}_T$	$]$
	$[\tau^+\tau^-$		e^+e^-	$\not{E}_T$	$]$
Inv. prod.					jj

of muons, for example, like-sign dimuons and three or four final state muons. If the $\tilde{\chi}_1^0$ decays only into $\tilde{\tau}_1\tau$, there are two signatures including like-sign dimuons for $\tilde{\mu}_L$ production. For $\tilde{\nu}_\mu$ production, muons can be produced singly only. But if the decays Eq. (4.4) are open, both slepton production processes allow for dimuon and trimuon production. In the case of $\tilde{\mu}_L$ production, even four final state muons are possible. Additionally, depending on how easily taus will be identified, an analysis could be based on like-sign $\mu\tau$ pairs.

The final state signatures depend sensitively on which particle is the LSP. Compared to slepton production in the $\tilde{\chi}_1^0$ LSP scenarios [52–56,60,61,63,64], there are three main differences here. First, for a $\tilde{\tau}_1$ LSP we have always one or two taus in the final state, which in $\tilde{\chi}_1^0$ LSP scenarios is only possible for smuon production if heavier neutralinos are involved in the decay chain. These heavy neutralinos then decay into the lightest neutralino and possibly taus. Second, the generation of a λ coupling can be neglected in $\tilde{\chi}_1^0$ LSP scenarios. As argued above, λ only allows for additional 3-body decays, which are thus not phase-space enhanced compared to the 3-body decays via the dominant λ' coupling. As a consequence, purely leptonic final state signatures are absent in $\tilde{\chi}_1^0$ LSP scenarios. Third, due to the modified spectra in $\tilde{\chi}_1^0$ LSP scenarios, also $\tilde{\nu}_\mu$ production can provide like-sign dimuon events. In this case, $\tilde{\nu}_\mu$ can often decay into a μ and a chargino. Like-sign dimuons arise either if the chargino directly decays via λ' into a μ and two quarks, or if the chargino first decays into the $\tilde{\chi}_1^0$ LSP and then the $\tilde{\chi}_1^0$ LSP decays via λ' into a μ and two quarks.

This discussion can easily be translated to scenarios with $\lambda'_{1jk} \neq 0$ by replacing the muons by electrons (and *vice versa*). Since there is typically no difference in mass between sleptons of the first and second generation, respectively, the kinematics are the same. Note however that the bounds on the B_3 couplings are stronger for λ'_{1jk} than for λ'_{2jk} for example due to the nonobservation of neutrinoless double beta decays.

C. $\lambda'_{3jk} \neq 0|_{\mathrm{GUT}}$

Some additional remarks are in order for a dominant λ'_{3jk} B_3 coupling. These couplings allow for resonant single $\tilde{\nu}_\tau$ production and, owing to the L–R mixing in the stau sector, also both resonant $\tilde{\tau}_1$ and $\tilde{\tau}_2$ production ($j \neq 3$).

For $\tilde{\tau}_1$ production, we refer to the discussion of LSP decay modes in Sec. III A. Here, the LSP couples directly to the B_3 operator and the inverse production process dominates the decay rate

$$\bar{u}_j d_k \to \tilde{\tau}_1^- \to \bar{u}_j d_k. \tag{4.6}$$

This decay is kinematically accessible if $j \neq 3$. For $j = 3$ the stau decays via a virtual top quark, cf. Eq. (3.6), for $m_{\tilde{\tau}_1} < m_t$. Note that $j = 3$ requires associated production, e.g. $g d_k \to \tilde{\tau} t$, due to the absence of top quarks inside the proton [50,69–71].

For $\tilde{\tau}_2$ and $\tilde{\nu}_\tau$ production, there are the following 2-body decay modes:

$$\bar{u}_j d_k \to \tilde{\tau}_2^- \to \begin{cases} \bar{u}_j d_k, \\ \tau^- \tilde{\chi}_1^0, \\ \tilde{\tau}_1^- h^0/Z^0, \end{cases} \tag{4.7}$$

$$\bar{d}_j d_k \to \tilde{\nu}_\tau \to \begin{cases} \bar{d}_j d_k, \\ \nu_\tau \tilde{\chi}_1^0, \\ \tilde{\tau}_1^- W. \end{cases} \tag{4.8}$$

The inverse production process contributes and leads to a jj final state. The decay into a lepton and a neutralino often dominates for small $\tan\beta$ ($\tan\beta \lesssim 10$). The neutralino decays further into the $\tilde{\tau}_1$ LSP, which directly decays into two quarks:

$$\tilde{\chi}_1^0 \to \tau^\pm \tilde{\tau}_1^\mp, \qquad \tilde{\tau}_1^- \to \bar{u}_j d_k, \tag{4.9}$$

where we have included the two charge conjugated decays of the neutralino. The final states of these decay modes are $\tau^-\tau^\pm jj$, and there is the possibility of like-sign tau events. If the $\tilde{\chi}_1^0$ decay (4.4) is kinematically allowed, we can have an additional pair of electrons or muons in the final state.

The singly produced slepton can also decay into the $\tilde{\tau}_1$ LSP and a SM particle, Z^0, h^0, or W, respectively, (final states: $h^0/Z^0/Wjj$). This decay mode is special for singly produced sleptons of the third generation because they are L–R mixed eigenstates. It can be the dominant decay mode of the $\tilde{\tau}_2$ and $\tilde{\nu}_\tau$, depending on the parameters.

The branching ratios for all B_3 conserving $\tilde{\tau}_2$ and $\tilde{\nu}_\tau$ 2-body decay modes are given in Table XI in Appendix B, for the SUSY parameter Sets A and B.

V. SINGLE-SMUON PRODUCTION: AN EXPLICIT NUMERICAL EXAMPLE

In this section, we present explicit calculations of promising signal rates for resonant slepton production at the LHC in the B_3 mSUGRA model with a $\tilde{\tau}_1$ LSP, focussing on parameter Sets A and B, cf. Eq. (2.7). First, we consider in Sec. V A (exclusive) like-sign dimuon events, i.e. events with exactly two muons of the same charge in the final state. An analysis of SM and SUSY backgrounds for the like-sign dimuon signature is given in Sec. V B. Second, in Sec. V C, we present event rates for single-smuon production leading to three or four muons in the final states, which are kinematically accessible within Sets A and B.

A. Like-sign dimuon events

Following Refs. [52,53], we first concentrate on events with exclusive like-sign dimuons. Here, events with more than two muons are rejected. In this sense, in $\tilde{\tau}_1$ LSP

scenarios, only single-smuon production leads to exclusive like-sign dimuon pairs, cf. Table IV. It has been shown in Refs. [52,53] that this selection criterion enhances the signal to background ratio considerably. In Refs. [52,53] it was shown that using a set of cuts, the SM background rate at the LHC, $\Gamma_B|_{\rm SM}$, can be reduced to

$$\Gamma_B|_{\rm SM} = 4.9 \pm 1.6 \text{ events}/10 \text{ fb}^{-1}. \quad (5.1)$$

At the same time the cut efficiency, i.e. the number of signal events that pass the cuts, lies roughly between 20% and 30%. Note that Refs. [52,53] assume a $\tilde{\chi}_1^0$ LSP. As we will argue in Sec. V B, similar cuts are also applicable in $\tilde{\tau}_1$ LSP scenarios. For the numbers presented in this section, however, no cuts are applied and full cross sections and event rates are given.

The total cross section for like-sign dimuon events is given by the resonant $\tilde{\mu}_L^+$ or $\tilde{\mu}_L^-$ production cross section multiplied by the respective branching ratios leading to like-sign dimuon final states. Both decays via the dominant λ'_{2jk} coupling and a generated λ_{233} coupling contribute. For a negatively charged smuon they are

$$\begin{aligned} \bar{u}_j d_k \xrightarrow{\lambda'} \tilde{\mu}_L^- \to \mu^- \tilde{\chi}_1^0, \\ \hookrightarrow \tau^+ \tilde{\tau}_1^- \\ \xhookrightarrow{\lambda'} \tau^- \mu^- u_j \bar{d}_k, \\ \xhookrightarrow{\lambda} \nu_\tau \mu^-, \\ \hookrightarrow \tau^- \tilde{\tau}_1^+ \\ \xhookrightarrow{\lambda'} \tau^+ \mu^- u_j \bar{d}_k, \end{aligned} \quad (5.2)$$

plus the analogous decay chains where the neutralino decays first into an $\tilde{e}_R^\mp$-$e^\mp$ pair, cf. Eq. (4.4). The couplings depicted on the arrows indicate the employed B_3 coupling. The decay chain for a positively charged smuon can be obtained by charge conjugation. However, one should keep in mind that the production cross sections for $\tilde{\mu}_L^+$ and $\tilde{\mu}_L^-$ differ at pp colliders, since charge conjugated quarks (and corresponding parton densities) are involved.

TABLE V. Cross sections for exclusive like-sign dimuon ($\mu^-\mu^-$ or $\mu^+\mu^+$) final states at the LHC within Set A. In the left column, we present the single-smuon production cross sections, $\sigma_{\rm prod.}(\tilde{\mu}_L^\mp)$, see also Tables IX and X. In the right column, we have folded in the relevant decay branching ratios, in order to obtain like-sign dimuons. All cross sections are given in femtobarn (fb). Where they exist, we have assumed always a cascade of 2-body decays. We consider in turn quark mixing in the up- and down-sector, when determining the dominant $\tilde{\tau}_1$ decay mode. The $\tilde{\tau}_1$ LSP can either decay via λ' (4-body decay) or via λ (2-body decay), cf. Table III, which leads to different like-sign dimuon cross sections, $\sigma_{\rm prod.} \times {\rm BR}_{\lambda'}$ and $\sigma_{\rm prod.} \times {\rm BR}_{\lambda}$, respectively. The λ'_{2jk} couplings are in accordance with neutrino mass bounds [10,96]. In case of up-type mixing, larger values of λ'_{2jk} for the four considered couplings are allowed by the neutrino mass bounds. The cross sections scale with $|\lambda'|^2$ and the corresponding rescaling can easily be performed.

Set A			Up-type mixing		Down-type mixing	
		$\sigma_{\rm prod.}(\tilde{\mu}_L^\mp)$ [fb]	$\sigma_{\rm prod.} \times {\rm BR}_{\lambda'}$	$\sigma_{\rm prod.} \times {\rm BR}_{\lambda}$	$\sigma_{\rm prod.} \times {\rm BR}_{\lambda'}$	$\sigma_{\rm prod.} \times {\rm BR}_{\lambda}$
$\lambda'_{211} = 2 \times 10^{-3}\vert_{\rm GUT}$	$\mu^-\mu^-$	61.6	11.1	0.71	9.81	2.09
	$\mu^+\mu^+$	108	19.4	1.25	17.2	3.66
$\lambda'_{221} = 2 \times 10^{-3}\vert_{\rm GUT}$	$\mu^-\mu^-$	42.0	7.84	-	4.51	3.88
	$\mu^+\mu^+$	16.2	3.03	-	1.74	1.50
$\lambda'_{212} = 2 \times 10^{-3}\vert_{\rm GUT}$	$\mu^-\mu^-$	18.6	3.46	-	1.99	1.71
	$\mu^+\mu^+$	86.0	16.1	-	9.23	7.94
$\lambda'_{213} = 2 \times 10^{-3}\vert_{\rm GUT}$	$\mu^-\mu^-$	8.80	1.67	-	1.32	0.40
	$\mu^+\mu^+$	49.8	9.43	-	7.43	2.24

TABLE VI. Same as Table V but for single slepton production within Set B. The neutrino mass bounds are less restrictive in the case of Set B, and $\lambda'_{2jk} = 0.01|_{\rm GUT}$ are considered for both up- and down-type quark mixing. All cross sections are given in fb.

Set B			Up-type mixing		Down-type mixing	
		$\sigma_{\rm prod.}(\tilde{\mu}_L^\mp)$ [fb]	$\sigma_{\rm prod.} \times {\rm BR}_{\lambda'}$	$\sigma_{\rm prod.} \times {\rm BR}_{\lambda}$	$\sigma_{\rm prod.} \times {\rm BR}_{\lambda'}$	$\sigma_{\rm prod.} \times {\rm BR}_{\lambda}$
$\lambda'_{211} = 1 \times 10^{-2}\vert_{\rm GUT}$	$\mu^-\mu^-$	476	1.04	101	0.21	102
	$\mu^+\mu^+$	885	1.93	188	0.39	189
$\lambda'_{221} = 1 \times 10^{-2}\vert_{\rm GUT}$	$\mu^-\mu^-$	309	62.8	-	-	66.2
	$\mu^+\mu^+$	105	21.4	-	-	22.5
$\lambda'_{212} = 1 \times 10^{-2}\vert_{\rm GUT}$	$\mu^-\mu^-$	123	25.1	-	-	26.3
	$\mu^+\mu^+$	681	139	-	-	146
$\lambda'_{213} = 1 \times 10^{-2}\vert_{\rm GUT}$	$\mu^-\mu^-$	54.6	11.2	-	0.02	11.7
	$\mu^+\mu^+$	370	75.6	-	0.16	79.4

The cross sections for the exclusive like-sign dimuon final states are presented in Table V for Set A and in Table VI for Set B. The smuon production cross sections, $\sigma_{\text{prod.}}(\tilde{\mu}_L^{\mp})$ (see also Tables IX and X), include NLO QCD and SUSY-QCD corrections [67], see Appendix A. For the numerical analysis, we only consider couplings λ'_{2jk} that involve partons of the first generation leading to large production cross sections at the LHC.

As already discussed, the $\tilde{\tau}_1$ LSP can either decay via λ' (4-body decay) or via λ (2-body decay). A list of the respective branching ratios is given in Appendix A, Tables XII and XIII, for Sets A and B and for several λ'_{2jk} couplings. Here, we show the resulting cross section times branching ratio, $\sigma_{\text{prod.}} \times \text{BR}_{\lambda'}$ and $\sigma_{\text{prod.}} \times \text{BR}_{\lambda}$, for like-sign dimuon events involving $\tilde{\tau}_1$ decays via λ' and λ, respectively, as described in Eq. (5.2).

The total number of exclusive like-sign dimuon events is given by the integrated luminosity multiplied by the total cross section. In Set A with up-type (down-type) quark mixing, we obtain per 10 fb^{-1}

$$N(\mu^-\mu^- + \mu^+\mu^+)/10\ \text{fb}^{-1} = [\sigma_{\text{prod.}}(\tilde{\mu}_L^-) + \sigma_{\text{prod.}}(\tilde{\mu}_L^+)] \times [\text{BR}_{\lambda'} + \text{BR}_{\lambda}] \times 10$$
$$\approx \begin{cases} 325 & (330) \\ 110 & (115) \\ 195 & (210) \\ 110 & (115) \end{cases} /10\ \text{fb}^{-1} \quad \text{for} \quad \begin{cases} \lambda'_{211} & = 0.002|_{\text{GUT}} \\ \lambda'_{221} & = 0.002|_{\text{GUT}} \\ \lambda'_{212} & = 0.002|_{\text{GUT}} \\ \lambda'_{213} & = 0.002|_{\text{GUT}} \end{cases}. \tag{5.3}$$

Note that for up-type mixing, some larger couplings may be considered. From the neutrino mass bounds, also $\lambda'_{211,221,212,213} = 0.01|_{\text{GUT}}$ (and even larger) are allowed. The cross sections are proportional to $|\lambda'|^2$ and thus a 5 times larger coupling implies cross sections and event numbers multiplied by a factor of 25 compared to those of Table V.

For Set B, $\lambda'_{2jk} = 0.01|_{\text{GUT}}$ is allowed for both up- and down-type mixing. The numbers of like-sign dimuon events are

$$N(\mu^-\mu^- + \mu^+\mu^+)/10\ \text{fb}^{-1} \approx \begin{cases} 2920 & (2920) \\ 840 & (890) \\ 1640 & (1720) \\ 870 & (910) \end{cases} /10\ \text{fb}^{-1} \quad \text{for} \quad \begin{cases} \lambda'_{211} & = 0.01|_{\text{GUT}} \\ \lambda'_{221} & = 0.01|_{\text{GUT}} \\ \lambda'_{212} & = 0.01|_{\text{GUT}} \\ \lambda'_{213} & = 0.01|_{\text{GUT}} \end{cases}, \tag{5.4}$$

for up-type (down-type) quark mixing, respectively.

As can be seen in Eqs. (5.3) and (5.4), for each nonzero λ' coupling the total event numbers for up- and down-mixing are of the same order. But as Tables V and VI show, the parts contributing to the event rate can be quite different. In case of up-type mixing and $j \neq k$, the 4-body decays via λ' dominate and the contributions of the 2-body decay are negligible [since the size of the necessary λ coupling is proportional to $(\mathbf{Y}_D)_{jk}$]. In contrast, for down-type mixing all four considered couplings can generate a relatively large λ_{233}, cf. Fig. 2, and the 2-body decay modes contribute considerably. In Set B, where $\tan\beta$ is large and where thus the fraction of 2-body decays is especially high (see discussion of Fig. 6), reliable event numbers are only obtained if the generation of λ_{233} is included in the theoretical framework. Moreover, a measurement of the ratio of 2-body to 4-body $\tilde{\tau}_1$ decays can reveal information about where the quark mixing takes place.

For $j = k$, the generation of a λ coupling is also possible in case of up-type mixing. In Set A, the generated λ_{233} is not large enough to allow for large 2-body decay rates. However in Set B, due to the large $\tan\beta$ value, the 2-body decays dominate over the 4-body decays. Thus, the different $\tilde{\tau}_1$ decay modes contain also information about $\tan\beta$.

We present in Tables V and VI also the total hadronic cross sections for single-smuon production, $\sigma_{\text{prod.}}(\tilde{\mu}_L^{\mp})$. Within one parameter set, the cross sections vary strongly for different λ'_{2jk}. This is of course related to corresponding required parton density functions. The largest cross section is obtained for $\lambda'_{211} \neq 0$, i.e. for the processes $\bar{u}d \to \tilde{\mu}_L^-$ and $u\bar{d} \to \tilde{\mu}_L^+$. Smaller cross sections are obtained for $\lambda'_{212} \neq 0$ (involving an up quark and a strange quark) and the smallest cross section for $\lambda'_{221} \neq 0$ (charm quark and down quark) and $\lambda'_{213} \neq 0$ (up quark together with bottom quark).

Since the LHC is a pp collider, there is an asymmetry between the $\tilde{\mu}_L^+$ and $\tilde{\mu}_L^-$ production cross sections. If experimentally a distinction between $\mu^+\mu^+$ and $\mu^-\mu^-$ event rates is found, the ratio can be used to constrain the indices of the nonzero λ'_{2jk} coupling. For example, a nonvanishing coupling λ'_{211} leads to a ratio of $N(\mu^+\mu^+):N(\mu^-\mu^-) \sim 2{:}1$ in Sets A and B, whereas for nonvanishing λ'_{221} the ratio is 1:2.5 in Set A and 1:3 in Set B. The highest event rates are obtained for processes that involve the valence quarks u and d. The charge con-

jugated processes, involving $\bar{u}$ or $\bar{d}$, are suppressed in comparison. Thus, a larger fraction of $\mu^+\mu^+$ events goes along with $j = 1$ (where the production process is $u\bar{d}_k \to \tilde{\mu}_L^+$) and a larger fraction of $\mu^-\mu^-$ events is related to $k = 1$ and $j \neq 1$ (production process $\bar{u}_j d \to \tilde{\mu}_L^-$).

B. Discussion of background and cuts for like-sign dimuon final states

In this section, we discuss the background for like-sign dimuon events from the SM and from SUSY particle pair production via gauge interactions. We follow Refs. [52,53] closely. There, single-smuon production via λ'_{211} was investigated assuming a $\tilde{\chi}_1^0$ LSP. A detailed signal over background analysis was performed based on like-sign dimuon events. We argue that a similar or even the same set of cuts might be used to suppress the background in our case, and we compare background and signal rates to determine the discovery potential of our analysis.

The main SM background sources are $t\bar{t}$ production, $b\bar{b}$ production, single top production, and gauge boson pair production, i.e. WW, WZ, and ZZ production. In Refs. [52,53], the dominant signature from single-smuon production including like-sign dimuon events is

$$\tilde{\mu}_L^- \to \mu^- \tilde{\chi}_1^0 \to \mu^-(\mu^- u\bar{d}). \tag{5.5}$$

The two muons of the signal (5.5) are isolated because they stem from different decays of SUSY particles. In addition, the muons carry large momenta since they originate from the decay of (heavy) SUSY particles. The following cuts were proposed to improve the signal over SM background ratio at the LHC:

(i) the muon rapidity $|\eta| < 2.0$, thus requiring all the leptons in the central region of the detector,
(ii) a cut on the transverse momentum on each muon: $p_T|_\mu \geq 40$ GeV,
(iii) an isolation cut on each of the muons,
(iv) a cut on the transverse mass of each of the muons, $60\ \text{GeV} < M_T < 85\ \text{GeV}$,
(v) a veto on the presence of a muon with the opposite charge as the like-sign dimuons,
(vi) a cut on the missing transverse energy, $\not{E}_T \leq 20$ GeV.

These cuts reduce the SM background to 4.9 ± 1.6 events per 10 fb^{-1} at the LHC, cf. Eq. (5.1). Among the above cuts, the isolation and p_T cut lead to the strongest suppression of the SM background.

We now investigate the case of a $\tilde{\tau}_1$ LSP. If the 4-body decays (3.3) of the $\tilde{\tau}_1$ LSP dominate, the leading signature of resonant single-smuon production including like-sign dimuon events can be written as

$$\tilde{\mu}_L^- \to \mu^- \tilde{\chi}_1^0 \to \mu^- \tau^\mp \tilde{\tau}^\pm \to \mu^- \tau^\mp(\tau^\pm \mu^- u\bar{d}). \tag{5.6}$$

As above, the muons originate from the decay of heavy particles ($\tilde{\tau}_1$ and $\tilde{\mu}_L$), are in general well isolated, and carry large momenta. Thus, for both signals Eqs. (5.5) and (5.6), the same cuts should allow to discriminate between the signal and the SM background. Furthermore, the additional pair of taus in Eq. (5.6) allows to require one or two (isolated!) taus. This might additionally improve the signal to background ratio.

If the $\tilde{\tau}_1$ LSP predominantly decays via 2-body decay modes, Eq. (3.4), the situation is a bit different. The like-sign dimuon signature is now

$$\tilde{\mu}_L^- \to \mu^- \tilde{\chi}_1^0 \to \mu^- \tau^+ \tilde{\tau}^- \to \mu^- \tau^+(\mu^- \nu_\tau). \tag{5.7}$$

We again have two isolated muons with large momenta, and the same isolation and $p_T|_\mu$ cuts as before should be useful to suppress the SM background. But the neutrino of the $\tilde{\tau}_1$ decay leads to high missing transverse energy $\not{E}_T$ in the signal and an upper bound on $\not{E}_T$ is not appropriate anymore. Alternatively, we propose a cut that requires a minimum missing energy, e.g. $\not{E}_T \geq 60$ GeV. This would also reduce the SM background where the main source of $\not{E}_T$ are low-energetic neutrinos from W decays. Furthermore, we can again require an additional tau in the final state. Finally, one can exploit the fact that the 2-body decays lead to a pure leptonic final state and a jet veto can be applied.

In Refs. [52,53], the SUSY background on like-sign dimuon events is suppressed by vetoing all events with more than two jets of $p_T|_{\text{jet}} > 50$ GeV. This cut will also work if the 4-body decay mode of the $\tilde{\tau}_1$ LSP (3.3) dominates. The 2-body decay modes lead to purely leptonic final states and even no high-p_T jet may be required.

We conclude that for $\tilde{\tau}_1$ LSP scenarios, the background for like-sign dimuon events can be suppressed similarly as it has been proposed for $\tilde{\chi}_1^0$ LSP scenarios in [52,53].

We thus compare our signal, as given in Eqs. (5.3) and (5.4) for Sets A and B, respectively, to the background, assuming that cuts as discussed above reduce the SM background to less than 5 events per 10 fb^{-1}, cf. Eq. (5.1). For the signal efficiency, we assume 20%, i.e. 20% of signal events pass the cuts. We neglect systematic errors, at this stage of the analysis.

For Set A, a more than 5σ excess over the SM background can be obtained for an integrated luminosity of 10 fb^{-1} for all couplings given in Eq. (5.3). For Set B, a cut efficiency of 20% for the signal corresponds to an excess between 100σ and 300σ for the number of like-sign muon events over the SM background! Therefore, within Set B, couplings can be tested at the LHC down to $\lambda'_{2jk}|_{\text{GUT}} \sim \mathcal{O}(10^{-3})$. But a detailed Monte Carlo based signal over background analysis remains to be done.

C. Final states with 3 and 4 muons

To round off our studies, we consider in this section final states with more than two muons. For example, for pa-

rameter Sets A and B, the $\tilde{\chi}_1^0$ cannot only decay into a $\tilde{\tau}_1$-τ pair but also into a $\tilde{\mu}_R$-μ or $\tilde{e}_R$-e pair. These are kinematically accessible and have non-negligible branching ratios (Set A: 7.0%, Set B: 2.2%; see Table XI). As we have shown in Table IV, these decays lead to three or even four muons of mixed signs in the final state. Each of the muons stems from the decay of a different SUSY particle. Especially the four-muon final state cannot be found at a high rate in $\tilde{\chi}_1^0$ LSP scenarios, and its observation could be a hint for a $\tilde{\tau}_1$ LSP. Therefore, we analyze the three- and four-muon final states in this section. All necessary branching ratios and production cross sections are given in the Appendix, see Tables IX, X, XI, XII, and XIII.

The four-muon events may be classified into $\mu^-\mu^-\mu^-\mu^+$, $\mu^-\mu^-\mu^+\mu^+$, and $\mu^-\mu^+\mu^+\mu^+$ signatures and we introduce the notations $\sigma(---+)$, $\sigma(--++)$, and $\sigma(+++-)$, for the respective cross sections. The four-muon final states require a long decay chain, and many different decays contribute at various stages. For smuon production, summing up all contributions, the cross sections can be written in the following compact form:

$$\begin{aligned}\sigma_{\tilde{\mu}}(---+) &= \sigma_{\text{prod.}}(\tilde{\mu}_L^-) \times \text{BR}(\tilde{\mu}_L^- \to \tilde{\chi}_1^0 \mu^-) \\ &\quad \times \text{BR}(\tilde{\chi}_1^0 \to \tilde{\mu}_R^+ \mu^-) \times P_{\tilde{\tau}_1}(1\mu), \\ \sigma_{\tilde{\mu}}(+++-) &= \sigma_{\tilde{\mu}}(---+) \times \sigma_{\text{prod.}}(\tilde{\mu}_L^+)/\sigma_{\text{prod.}}(\tilde{\mu}_L^-), \\ \sigma_{\tilde{\mu}}(--++) &= \sigma_{\tilde{\mu}}(---+) + \sigma_{\tilde{\mu}}(+++-), \end{aligned} \tag{5.8}$$

where $P_{\tilde{\tau}_1}(1\mu) = \text{BR}(\tilde{\tau}_1^- \to \mu^- \ldots) + \text{BR}(\tilde{\tau}_1^+ \to \mu^- \ldots)$ denotes the probability of a negatively charged final state muon in a $\tilde{\tau}_1$ decay. The difference between $\sigma_{\tilde{\mu}}(---+)$ and $\sigma_{\tilde{\mu}}(+++-)$ stems from the different partons and parton densities involved in the production cross sections.

Smuon production can also lead to exactly three final state charged muons, $\mu^-\mu^-\mu^+$ or $\mu^+\mu^+\mu^-$. The corresponding cross sections now involve the probability $P_{\tilde{\tau}_1}(0\mu)$ for a $\tilde{\tau}_1$ decay without a final state muon,

$$\begin{aligned}\sigma_{\tilde{\mu}}(--+) &= \sigma_{\text{prod.}}(\tilde{\mu}_L^-) \times \text{BR}(\tilde{\mu}_L^- \to \tilde{\chi}_1^0 \mu^-) \\ &\quad \times \text{BR}(\tilde{\chi}_1^0 \to \tilde{\mu}_R^+ \mu^-) \times 2P_{\tilde{\tau}_1}(0\mu), \\ \sigma_{\tilde{\mu}}(++-) &= \sigma_{\tilde{\mu}}(--+) \times \sigma_{\text{prod.}}(\tilde{\mu}_L^+)/\sigma_{\text{prod.}}(\tilde{\mu}_L^-). \end{aligned} \tag{5.9}$$

There are 16 different decay chains of the $\tilde{\mu}_L^-$ leading to a $\mu^-\mu^-\mu^+$ final state. The factor of 2 in Eq. (5.9) is a consequence of summing over all these decay chains.

The same final state signatures (exactly three muons) can be obtained via $\tilde{\nu}_\mu$ production. The decay chain is similar to that of a produced smuon. The missing muon from the slepton decay is here replaced by demanding a muon in the final $\tilde{\tau}_1$ decay,

$$\begin{aligned}\sigma_{\tilde{\nu}}(--+) &= [\sigma_{\text{prod.}}(\tilde{\nu}_\mu) + \sigma_{\text{prod.}}(\tilde{\nu}_\mu^*)] \\ &\quad \times \text{BR}(\tilde{\nu}_\mu \to \tilde{\chi}_1^0 \nu_\mu) \\ &\quad \times \text{BR}(\tilde{\chi}_1^0 \to \tilde{\mu}_R^+ \mu^-) \times P_{\tilde{\tau}_1}(1\mu), \\ \sigma_{\tilde{\nu}}(++-) &= \sigma_{\tilde{\nu}}(--+). \end{aligned} \tag{5.10}$$

The total cross sections for (exactly) three final state muons are then given by

$$\sigma(\mp\mp\pm) = \sigma_{\tilde{\mu}}(\mp\mp\pm) + \sigma_{\tilde{\nu}}(\mp\mp\pm). \tag{5.11}$$

Tables VII and VIII give an overview over the numerical results. The same λ' couplings as in the previous Tables V and VI are considered. The generation of λ_{233} has been taken into account for the $\tilde{\tau}_1$ decays and the cross sections give total numbers, including both 4- and 2-body $\tilde{\tau}_1$ decays.

We see that the sum of three- and four-muon events is in the same order of magnitude as the results for purely like-sign dimuons. For Set A, where $\text{BR}(\tilde{\chi}_1^0 \to \tilde{\mu}_R \mu) = 7\%$,

TABLE VII. Cross sections for signals with three or four final state muons within parameter Set A, assuming down-type (up-type) quark mixing. Given are the cross sections as defined in Eqs. (5.8), (5.9), (5.10), and (5.11) and the sums for two negatively or positively charged muons, $\sum \sigma(--\ldots)$ or $\sum \sigma(++\ldots)$, respectively. All cross sections are given in fb.

Set A	$\sigma(--+)$	$\sigma(++-)$	$\sigma(--++)$	$\sigma(+++-)$	$\sigma(---+)$	$\sum\sigma(--\ldots)$	$\sum\sigma(++\ldots)$
$\lambda'_{211} = 2\times10^{-3}\vert_{\text{GUT}}$	9.38 (9.39)	12.9 (13.0)	5.32 (5.26)	3.39 (3.35)	1.93 (1.91)	16.6 (16.6)	21.7 (21.6)
$\lambda'_{221} = 2\times10^{-3}\vert_{\text{GUT}}$	5.77 (5.77)	3.84 (3.74)	1.89 (1.77)	0.53 (0.49)	1.36 (1.27)	9.02 (8.81)	6.26 (6.00)
$\lambda'_{212} = 2\times10^{-3}\vert_{\text{GUT}}$	4.02 (3.93)	9.05 (9.24)	3.39 (3.17)	2.79 (2.61)	0.60 (0.56)	8.01 (7.66)	15.2 (15.0)
$\lambda'_{213} = 2\times10^{-3}\vert_{\text{GUT}}$	2.04 (2.02)	5.14 (5.19)	1.85 (1.80)	1.57 (1.53)	0.28 (0.27)	4.17 (4.09)	8.56 (8.52)

TABLE VIII. Same as Table VII but for single slepton production within Set B. All cross sections are given in fb.

Set B	$\sigma(--+)$	$\sigma(++-)$	$\sigma(--++)$	$\sigma(+++-)$	$\sigma(---+)$	$\sum\sigma(--\ldots)$	$\sum\sigma(++\ldots)$
$\lambda'_{211} = 1\times10^{-2}\vert_{\text{GUT}}$	20.8 (20.8)	29.1 (29.1)	13.4 (13.4)	8.73 (8.73)	4.69 (4.69)	38.9 (38.9)	51.3 (51.3)
$\lambda'_{221} = 1\times10^{-2}\vert_{\text{GUT}}$	11.9 (12.0)	7.77 (7.59)	4.08 (3.88)	1.04 (0.98)	3.05 (2.89)	19.1 (18.7)	12.9 (12.4)
$\lambda'_{212} = 1\times10^{-2}\vert_{\text{GUT}}$	8.14 (7.98)	19.5 (19.9)	7.93 (7.53)	6.72 (6.39)	1.21 (1.15)	17.3 (16.7)	34.2 (33.8)
$\lambda'_{213} = 1\times10^{-2}\vert_{\text{GUT}}$	3.94 (3.85)	10.4 (10.6)	4.20 (4.00)	3.66 (3.48)	0.54 (0.51)	8.68 (8.36)	18.3 (18.1)

the event numbers are even larger. In Set B, with $\mathrm{BR}(\tilde{\chi}_1^0 \to \tilde{\mu}_R \mu) = 2\%$, the total contributions are smaller by a factor of about three. Depending on the experimental goals, these channels thus give important contributions and should be included in an analysis. On the other hand, these events also suggest to use three or four final state muons as a signal for slepton production, since the background is expected to be very low.

VI. CONCLUSION

B_3 interactions allow for LSP decays and thus reopen large regions in the SUSY parameter space, where the LSP is charged. We have investigated for the first time in detail the phenomenology of B_3 mSUGRA models with a $\tilde{\tau}_1$ LSP. We have hereby assumed only one nonvanishing B_3 coupling λ'_{ijk} at M_{GUT}.

An essential feature of the B_3 mSUGRA signatures is the decay of the $\tilde{\tau}_1$ LSP. Given only one B_3 coupling at M_{GUT}, we would expect either a 4-body or 2-body decay of the $\tilde{\tau}_1$ LSP depending on whether it couples directly to the dominant B_3 operator or not. However, in B_3 mSUGRA models the RGEs are highly coupled and further couplings are generated at the weak scale. These are of course suppressed relative to the dominant coupling but may lead to 2-body decays, which have larger phase space and do not involve heavy propagators.

We have here numerically investigated the generation of λ_{i33} couplings via dominant λ'_{ijk} couplings. The generated couplings are typically smaller by at least 2 orders of magnitude; see Figs. 2 and 3. We have then performed a first detailed analysis of the parameter dependence of the $\tilde{\tau}_1$ LSP decay modes. It turned out that in large regions of parameter space the 2-body decay dominates over the 4-body decay, see Figs. 6–10.

In the second part of the paper, we applied our results to resonant single slepton production at the LHC, which is possible in B_3 scenarios with a nonzero λ'_{ijk} coupling. We first studied the general decay signatures. From the experimental point of view, the final states with two like-sign or even more charged leptons are of special interest. Each event is also accompanied by at least one tau.

We further investigated numerically single-smuon production for $\lambda'_{2jk} \neq 0$ within two representative $\tilde{\tau}_1$ LSP scenarios, i.e. for two sets of B_3 mSUGRA parameters. We include the 2-body $\tilde{\tau}_1$ LSP decays via the generated λ_{233} couplings in our analysis. The cross sections for like-sign dimuon final states are given in Tables V and VI and those for final states with three or four muons in Tables VII and VIII. For example, we found resulting cross sections for exclusive like-sign dimuon events of $\mathcal{O}(100\ \mathrm{fb})$ for $\lambda'_{2jk}|_{\mathrm{GUT}} = 0.01$. Additional three- and four-muon events can occur with the same rate. This is a novel discovery mechanism for the LHC and should be investigated in more detail, also by the LHC experimental groups.

ACKNOWLEDGMENTS

We thank B. Allanach and M. Bernhardt for valuable help with the as-yet unpublished B_3 version of SOFTSUSY. S. G. thanks the theory groups of Fermilab National Accelerator, Argonne National Laboratory, and UC Santa Cruz for helpful discussions and warm hospitality. S. G. also thanks the "Deutsche Telekom Stiftung" and the "Bonn-Cologne Graduate School of Physics and Astronomy" for financial support. This work was partially supported by BMBF Grant No. 05 HT6PDA and by the Helmholtz Alliance HA-101 "Physics at the Terascale."

APPENDIX A: CROSS SECTIONS AND BRANCHING RATIOS RELEVANT FOR SLEPTON PRODUCTION AND DECAY

In this appendix we give the necessary cross sections and branching ratios to calculate rates of all possible decay signatures for single slepton production at the LHC, within the B_3 Sets A and B with a $\tilde{\tau}_1$ LSP, cf. Eq. (2.7).

In Tables IX and X, all hadronic production cross sections of resonant single sleptons within parameter Set A and Set B, respectively, are given. We consider here

TABLE IX. Complete list of hadronic cross sections for resonant single slepton/sneutrino production via $\lambda'_{ijk} = 0.01|_{\mathrm{GUT}}$ at the pp collider LHC ($\sqrt{S} = 14$ TeV) within the parameter Set A. The cross sections include QCD and SUSY-QCD corrections at NLO [67]. For λ'_{i3k}, sleptons cannot be produced because of the vanishing top-quark density in the proton.

	$\sigma_{\mathrm{prod.}}$ [fb]									
Set A	$\tilde{e}_L^+/\tilde{\mu}_L^+$	$\tilde{e}_L^-/\tilde{\mu}_L^-$	$\tilde{\nu}_{e/\mu}^*$	$\tilde{\nu}_{e/\mu}$	$\tilde{\tau}_2^+$	$\tilde{\tau}_2^-$	$\tilde{\tau}_1^+$	$\tilde{\tau}_1^-$	$\tilde{\nu}_\tau^*$	$\tilde{\nu}_\tau$
$\lambda'_{i11} = 0.01\|_{\mathrm{GUT}}$	2700	1540	1860	1860	2620	1500	434	272	190	190
$\lambda'_{i22} = 0.01\|_{\mathrm{GUT}}$	268	268	410	410	2600	2600	64.5	64.5	421	421
$\lambda'_{i12} = 0.01\|_{\mathrm{GUT}}$	2150	464	1430	602	2090	451	360	103	1460	616
$\lambda'_{i21} = 0.01\|_{\mathrm{GUT}}$	405	1050	602	1430	393	1020	91.9	197	616	1460
$\lambda'_{i13} = 0.01\|_{\mathrm{GUT}}$	1240	220	788	292	1210	214	216	51.3	806	299
$\lambda'_{i23} = 0.01\|_{\mathrm{GUT}}$	119	119	191	191	116	116	30.0	30.0	196	196
$\lambda'_{i31} = 0.01\|_{\mathrm{GUT}}$	-	-	247	666	-	-	-	-	253	681
$\lambda'_{i32} = 0.01\|_{\mathrm{GUT}}$	-	-	161	161	-	-	-	-	166	166
$\lambda'_{i33} = 0.01\|_{\mathrm{GUT}}$	-	-	69.3	69.3	-	-	–	-	71.1	71.1

TABLE X. Same as Table IX but for parameter Set B.

Set B	$\sigma_{\text{prod.}}$ [fb] $\tilde{e}_L^+/\tilde{\mu}_L^+$	$\tilde{e}_L^-/\tilde{\mu}_L^-$	$\tilde{\nu}_{e/\mu}^*$	$\tilde{\nu}_{e/\mu}$	$\tilde{\tau}_2^+$	$\tilde{\tau}_2^-$	$\tilde{\tau}_1^+$	$\tilde{\tau}_1^-$	$\tilde{\nu}_\tau^*$	$\tilde{\nu}_\tau$
$\lambda'_{i11} = 0.01\|_{\text{GUT}}$	885	476	559	559	949	515	1168	750	657	657
$\lambda'_{i22} = 0.01\|_{\text{GUT}}$	67.3	67.3	102	102	74.7	74.7	192	192	124	124
$\lambda'_{i12} = 0.01\|_{\text{GUT}}$	681	123	414	155	735	136	976	301	490	187
$\lambda'_{i21} = 0.01\|_{\text{GUT}}$	105	309	155	414	117	337	269	548	187	490
$\lambda'_{i13} = 0.01\|_{\text{GUT}}$	370	54.6	214	70.2	401	60.6	572	146	255	85.4
$\lambda'_{i23} = 0.01\|_{\text{GUT}}$	28.2	28.2	44.4	44.4	31.4	31.4	87.2	87.2	54.3	54.3
$\lambda'_{i31} = 0.01\|_{\text{GUT}}$	-	-	60.4	184	-	-	-	-	73.5	219
$\lambda'_{i32} = 0.01\|_{\text{GUT}}$	-	-	38.2	38.2	-	-	-	-	46.7	46.7
$\lambda'_{i33} = 0.01\|_{\text{GUT}}$	-	-	14.8	14.8	-	-	-	-	18.2	18.2

$\lambda'_{ijk} = 0.01|_{\text{GUT}}$, but the cross section scales with $|\lambda'_{ijk}|^2$. The running of λ'_{ijk} is taken into account according to Eq. (2.22), leading to the following values at the SUSY scale Q_{susy}, cf. Eq. (2.28):

$$\begin{aligned} \text{Set A: } \lambda'_{2jk} &= 0.0282, & \lambda'_{3jk} &= 0.0282, \\ \lambda'_{23k} &= 0.0258, & \lambda'_{33k} &= 0.0257, \\ \lambda'_{2j3} &= 0.0281, & \lambda'_{3j3} &= 0.0280, \\ \lambda'_{233} &= 0.0255, & \lambda'_{333} &= 0.0254; \end{aligned} \tag{A1}$$

$$\begin{aligned} \text{Set B: } \lambda'_{2jk} &= 0.0274, & \lambda'_{3jk} &= 0.0271, \\ \lambda'_{23k} &= 0.0249, & \lambda'_{33k} &= 0.0247, \\ \lambda'_{2j3} &= 0.0269, & \lambda'_{3j3} &= 0.0266, \\ \lambda'_{233} &= 0.0238, & \lambda'_{333} &= 0.0236, \end{aligned} \tag{A2}$$

where $j, k = 1, 2$ and $Q_{\text{susy}} = 893$ GeV for Set A and $Q_{\text{susy}} = 1209$ GeV for Set B.

The production cross sections include NLO SUSY-QCD corrections [67]. The latter depend on the trilinear quark-squark-slepton coupling, h_{D^k}, defined in Ref. [10]. Numerically, it is $h_{D^k} = -23.4$ GeV $(-21.2$ GeV) within Set A (Set B) at the SUSY scale. We incorporated the running of h_{D^k} by using the one-loop contributions from gauge interactions [10].

Second, for the calculation of the rate for a given signature of resonant single slepton production, the branching ratios for the slepton decay and for the subsequent decay chains down to the $\tilde{\tau}_1$ LSP are needed. For all dominant λ'_{ijk} couplings these branching ratios are universal within parameter Set A and Set B, respectively, and are given in Table XI.

Finally, we show in Table XII (Table XIII) all branching ratios of $\tilde{\tau}_1$ LSP decays for different couplings λ'_{2jk} at the GUT scale. Branching ratios within scenarios with $\lambda'_{1jk} \neq 0$ are analogous and can be obtained from the tables by replacing μ by e in the final state signatures.

In the case of a nonvanishing λ'_{3jk}, the $\tilde{\tau}_1$ LSP directly couples to the dominant $L_3 Q_j \bar{D}_k$ operator and decays predominantly via the inverse production process, see also the discussion in Sec. III A. For the special case of $\lambda'_{33k} \neq 0$ and $m_{\tilde{\tau}_1} < m_t$, however, the $\tilde{\tau}_1$ decays into a W boson and two jets, cf. Eq. (3.6). The corresponding matrix element and partial width are calculated in Appendix B.

TABLE XI. Table of branching ratios, BRs, that are relevant for single slepton production and decays within the B_3 mSUGRA scenarios Set A and Set B. Two different nonzero B_3 couplings are considered, $\lambda'_{2jk} = 0.01|_{\text{GUT}}$ for columns 2 and 3 and $\lambda'_{3jk} = 0.01|_{\text{GUT}}$ for columns 4 and 5. The branching ratios for $\lambda'_{1jk} \neq 0$ can be obtained from those for $\lambda'_{2jk} \neq 0$ by interchanging muon and electron flavor in the first four decay channels. The branching ratios for $\tilde{e}_L$ $(\tilde{\nu}_e, \tilde{e}_R)$ in scenarios with $\lambda'_{ijk} \neq 0$, $i \neq 1$ are equal to those of $\tilde{\mu}_L$ $(\tilde{\nu}_\mu, \tilde{\mu}_R)$ with $\lambda'_{3jk} \neq 0$. The branching ratios for $\tilde{\tau}_1$ LSP decays are listed separately in Tables XII and XIII.

	BRs [%] $\lambda'_{2jk} = 0.01\|_{\text{GUT}}$ Set A	Set B	$\lambda'_{3jk} = 0.01\|_{\text{GUT}}$ Set A	Set B
$\tilde{\mu}_L^- \to \tilde{\chi}_1^0 \mu^-$	91.1	91.3	100	100
$\tilde{\mu}_L^- \to \bar{u}_j d_k$	8.9	8.7	-	-
$\tilde{\nu}_\mu \to \tilde{\chi}_1^0 \nu_\mu$	91.7	91.5	100	100
$\tilde{\nu}_\mu \to \bar{d}_j d_k$	9.3	8.4	-	-
$\tilde{\chi}_1^0 \to \tilde{\tau}_1^\pm \tau^\mp$	36.0	45.7	36.0	45.7
$\tilde{\chi}_1^0 \to \tilde{\mu}_R^\pm \mu^\mp$	7.0	2.2	7.0	2.2
$\tilde{\chi}_1^0 \to \tilde{e}_R^\pm e^\mp$	7.0	2.1	7.0	2.1
$\tilde{\mu}_R^- \to \tilde{\tau}_1^+ \mu^- \tau^-$	54.3	64.1	54.3	64.1
$\tilde{\mu}_R^- \to \tilde{\tau}_1^- \mu^- \tau^+$	45.7	35.9	45.7	35.9
$\tilde{\tau}_2^- \to \tilde{\chi}_1^0 \tau^-$	58.4	14.7	55.5	14.5
$\tilde{\tau}_2^- \to \tilde{\tau}_1^- h^0$	22.5	41.8	21.4	41.2
$\tilde{\tau}_2^- \to \tilde{\tau}_1^- Z^0$	19.1	43.5	18.1	42.9
$\tilde{\tau}_2^- \to \bar{u}_j d_k$	-	-	5.0	1.3
$\tilde{\nu}_\tau \to \tilde{\chi}_1^0 \nu_\tau$	62.2	13.6	58.8	13.4
$\tilde{\nu}_\tau \to \tilde{\tau}_1^- W^+$	37.8	86.4	35.8	85.2
$\tilde{\nu}_\tau \to \bar{d}_j d_k$	-	-	5.4	1.4

TABLE XII. Branching ratios of the $\tilde{\tau}_1$ LSP for different nonzero λ'_{2jk} couplings at the GUT scale. The branching ratios are calculated within the mSUGRA parameter Set A for the SUSY breaking scale $Q_{\text{susy}} = 893$ GeV. We assume down-type (up-type) quark mixing. Branching ratios for nonvanishing λ'_{1jk} are analogous, with μ replaced by e.

Set A	$\tilde{\tau}_1^- \xrightarrow{\lambda} \nu_\mu \tau^-$ $[= \tilde{\tau}_1^- \xrightarrow{\lambda} \nu_\tau \mu^-]$		$\tilde{\tau}_1^- \xrightarrow{\lambda} \bar{\nu}_\mu \tau^-$		$\tilde{\tau}_1^- \xrightarrow{\lambda'} \tau^- \mu^- u_j \bar{d}_k$		$\tilde{\tau}_1^- \xrightarrow{\lambda'} \tau^- \mu^+ \bar{u}_j d_k$		$\tilde{\tau}_1^- \xrightarrow{\lambda'} \tau^- \nu_\mu d_j \bar{d}_k$		$\tilde{\tau}_1^- \xrightarrow{\lambda'} \tau^- \bar{\nu}_\mu \bar{d}_j d_k$	
λ'_{211}	7.9%	(2.7%)	0.2%	(0.1%)	11.8%	(13.3%)	25.3%	(28.5%)	15.2%	(17.1%)	31.6%	(35.6%)
λ'_{212}	21.5%	(-)	0.5%	(-)	7.9%	(14.2%)	17.1%	(29.3%)	10.2%	(18.1%)	21.3%	(38.4%)
λ'_{213}	10.5%	(-)	0.2%	(-)	11.1%	(14.1%)	23.8%	(30.2%)	14.3%	(18.1%)	29.6%	(37.6%)
λ'_{221}	21.5%	(-)	0.5%	(-)	7.9%	(14.2%)	17.1%	(29.3%)	10.2%	(18.1%)	21.3%	(38.4%)
λ'_{222}	46.8%	(46.8%)	1.1%	(1.1%)	0.7%	(0.8%)	1.6%	(1.6%)	1.0%	(1.0%)	2.0%	(2.0%)
λ'_{223}	48.2%	(-)	1.1%	(-)	0.4%	(14.2%)	0.8%	(29.3%)	0.5%	(18.2%)	1.0%	(38.4%)
λ'_{231}	17.9%	(-)	0.4%	(-)	-	(-)	-	(-)	20.7%	(32.1%)	43.0%	(67.9%)
λ'_{232}	48.8%	(-)	1.1%	(-)	-	(-)	-	(-)	0.4%	(32.5%)	0.8%	(67.5%)
λ'_{233}	49.4%	(49.4%)	1.1%	(1.1%)	-	(-)	-	(-)	-	(-)	-	(-)

TABLE XIII. Branching ratios of the $\tilde{\tau}_1$ LSP for different nonzero λ'_{2jk} couplings at the GUT scale. The branching ratios are calculated within the mSUGRA parameter Set B for the SUSY breaking scale $Q_{\text{susy}} = 1209$ GeV. We assume down-type (up-type) quark mixing. Branching ratios for nonvanishing λ'_{1jk} are analogous, with μ replaced by e.

Set B	$\tilde{\tau}_1^- \xrightarrow{\lambda} \nu_\mu \tau^-$ $[= \tilde{\tau}_1^- \xrightarrow{\lambda} \nu_\tau \mu^-]$		$\tilde{\tau}_1^- \xrightarrow{\lambda} \bar{\nu}_\mu \tau^-$		$\tilde{\tau}_1^- \xrightarrow{\lambda'} \tau^- \mu^- u_j \bar{d}_k$		$\tilde{\tau}_1^- \xrightarrow{\lambda'} \tau^- \mu^+ \bar{u}_j d_k$		$\tilde{\tau}_1^- \xrightarrow{\lambda'} \tau^- \nu_\mu d_j \bar{d}_k$		$\tilde{\tau}_1^- \xrightarrow{\lambda'} \tau^- \bar{\nu}_\mu \bar{d}_j d_k$	
λ'_{211}	49.0%	(48.6%)	1.7%	(1.7%)	-	(0.1%)	0.1%	(0.4%)	-	(0.1%)	0.1%	(0.5%)
λ'_{212}	49.1%	(-)	1.7%	(-)	-	(5.6%)	-	(41.1%)	-	(6.3%)	-	(46.9%)
λ'_{213}	49.0%	(-)	1.7%	(-)	-	(5.7%)	0.1%	(41.0%)	-	(6.4%)	0.1%	(46.9%)
λ'_{221}	49.1%	(-)	1.7%	(-)	-	(5.6%)	-	(41.0%)	-	(6.3%)	-	(47.0%)
λ'_{222}	49.1%	(49.1%)	1.7%	(1.7%)	-	(-)	-	(-)	-	(-)	-	(-)
λ'_{223}	49.1%	(-)	1.7%	(-)	-	(5.7%)	-	(41.0%)	-	(6.4%)	-	(47.0%)
λ'_{231}	49.1%	(-)	1.7%	(-)	-	(-)	-	(-)	-	(12.0%)	0.1%	(88.0%)
λ'_{232}	49.1%	(-)	1.7%	(-)	-	(-)	-	(-)	-	(12.0%)	-	(88.0%)
λ'_{233}	49.1%	(49.1%)	1.7%	(1.7%)	-	(-)	-	(-)	-	(-)	-	(-)

APPENDIX B: THE B_3 SLEPTON DECAY $\tilde{\ell}_i^- \to W^- \bar{b} d_k$

A nonvanishing $L_i Q_3 \bar{D}_k$ operator allows for slepton decay into a top quark t and a down-type quark d_k of generation k,

$$\tilde{\ell}_i^- \to \bar{t} d_k. \tag{B1}$$

However, this decay mode is kinematically only allowed if $m_{\tilde{\ell}_i} > m_t + m_{d_k}$. For $m_{\tilde{\ell}_i} < m_t + m_{d_k}$, the slepton decays via a virtual top quark,

$$\tilde{\ell}_i^- \to W^- \bar{b} d_k. \tag{B2}$$

This 3-body decay has not been considered in the literature yet and is not implemented in the R-parity violating version of HERWIG, either. We complete the picture by calculating the 3-body decay (B2) in the following.

The relevant parts of the supersymmetric Lagrangian are [100]

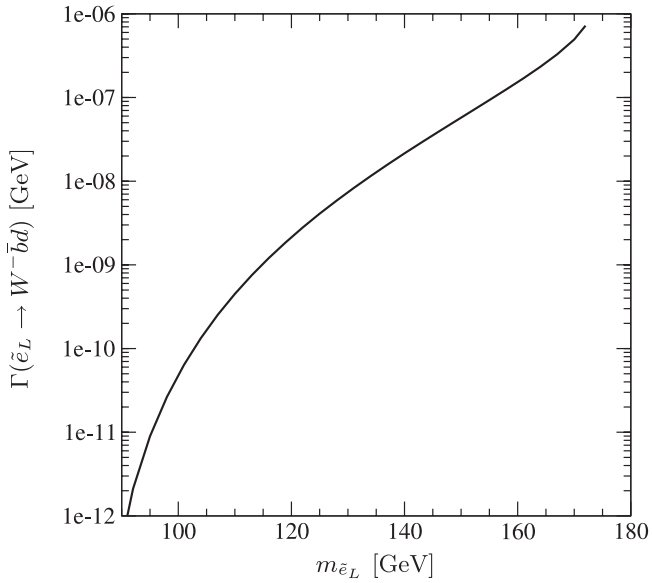

FIG. 13. Partial width in GeV for the 3-body decay $\tilde{e}_L \to W^- \bar{b} d$ as a function of the selectron mass $m_{\tilde{e}_L}$. We take $\lambda'_{131} = 0.01$ and $L_{11} = 1$, in Eq. (B4).

$$\mathcal{L}_{L_iQ_3\bar{D}_k} = \lambda'_{i3k} L_{1\beta} \tilde{\ell}^-_{i\beta} \bar{d}_k P_L t + \text{h.c.},$$
$$\mathcal{L}_{bWt} = -\frac{g}{\sqrt{2}} W^+_\mu \bar{t} \gamma^\mu P_L b + \text{h.c.}, \tag{B3}$$

where $L_{\alpha\beta}$ is the slepton mixing matrix, α the left-right eigenstate, and β the mass eigenstate. From Eq. (B3), the squared matrix element (summed over final state polarizations and colors) can be derived,

$$\begin{aligned}
&|\overline{M}(\tilde{\ell}^-_{i\beta} \to W^- \bar{b} d_k)|^2 \\
&= \frac{3}{2} \frac{\lambda'^2_{i3k} L^2_{1\beta} g^2}{[(W+b)^2 - m_t^2]^2 + m_t^2 \Gamma_t^2} \\
&\quad \times \left\{ 2(d_k \cdot b) \left[m_b^2 - m_W^2 + 4(W \cdot b) + \frac{4(W \cdot b)^2}{m_W^2} \right] \right. \\
&\quad \left. + 4(d_k \cdot W) \left[m_b^2 + 2(W \cdot b) - m_b^2 \frac{(W \cdot b)}{m_W^2} \right] \right\}.
\end{aligned} \tag{B4}$$

We denote the particle four-momenta by the particle letter, and m_t, m_b, and m_W, are the top, bottom, and W mass, respectively. Γ_t is the total width of the top quark.

From the squared matrix element (B4) we obtain easily the partial width for the 3-body decay (B2), see e.g. [100]. We show in Fig. 13 the partial width $\Gamma(\tilde{e}_L \to W^- \bar{b} d)$ as a function of the left-handed selectron mass $m_{\tilde{e}_L}$. Here, we take $\lambda'_{131} = 0.01$ and $L_{11} = 1$, in Eq. (B4).

In comparison to the 3-body decay (B2), the possible 4-body decays via λ'_{i3k} are negligible. For example, for the parameter Set B with nonvanishing λ'_{331}, the branching ratio of the 3-body $\tilde{\tau}_1$ LSP decay (B2) is larger by 5 orders of magnitude than the branching ratio of the 4-body $\tilde{\tau}_1$ LSP decays.

[1] J. Wess and B. Zumino, Nucl. Phys. **B70**, 39 (1974).
[2] M. Drees, arXiv:hep-ph/9611409.
[3] H. P. Nilles, Phys. Rep. **110**, 1 (1984).
[4] S. P. Martin, arXiv:hep-ph/9709356.
[5] S. L. Glashow, Nucl. Phys. **22**, 579 (1961).
[6] S. Weinberg, Phys. Rev. Lett. **19**, 1264 (1967).
[7] (ATLAS Collaboration), Report No. CERN-LHCC-94-43.
[8] (CMS Collaboration), Report No. CERN-LHCC-96-45.
[9] B. C. Allanach, M. A. Bernhardt, H. K. Dreiner, C. H. Kom, and P. Richardson, Phys. Rev. D **75**, 035002 (2007).
[10] B. C. Allanach, A. Dedes, and H. K. Dreiner, Phys. Rev. D **69**, 115002 (2004).
[11] L. E. Ibáñez and G. G. Ross, Phys. Lett. B **260**, 291 (1991).
[12] L. E. Ibáñez and G. G. Ross, Nucl. Phys. **B368**, 3 (1992).
[13] Y. Grossman and H. E. Haber, Phys. Rev. D **59**, 093008 (1999).
[14] H. Dreiner, C. Luhn, and M. Thormeier, Phys. Rev. D **73**, 075007 (2006).
[15] H. K. Dreiner, C. Luhn, H. Murayama, and M. Thormeier, Nucl. Phys. **B774**, 127 (2007).
[16] N. Sakai and T. Yanagida, Nucl. Phys. **B197**, 533 (1982).
[17] S. Weinberg, Phys. Rev. D **26**, 287 (1982).
[18] B. C. Allanach, A. Dedes, and H. K. Dreiner, Phys. Rev. D **60**, 075014 (1999).
[19] A. Y. Smirnov and F. Vissani, Phys. Lett. B **380**, 317 (1996).
[20] G. Bhattacharyya and P. B. Pal, Phys. Rev. D **59**, 097701 (1999).
[21] R. Barbier *et al.*, Phys. Rep. **420**, 1 (2005).
[22] Super-Kamiokande, M. Shiozawa *et al.*, Phys. Rev. Lett. **81**, 3319 (1998).
[23] S. Dimopoulos, S. Raby, and F. Wilczek, Phys. Lett. **112B**, 133 (1982).
[24] H.-S. Lee, K. T. Matchev, and T. T. Wang, Phys. Rev. D **77**, 015016 (2008).
[25] H.-S. Lee, C. Luhn, and K. T. Matchev, J. High Energy Phys. 07 (2008) 065.
[26] H.-S. Lee, Phys. Lett. B **663**, 255 (2008).
[27] H. K. Dreiner, arXiv:hep-ph/9707435.
[28] H. Dreiner and G. G. Ross, Nucl. Phys. **B365**, 597 (1991).
[29] B. Allanach *et al.* (R parity Working Group), arXiv:hep-ph/9906224.
[30] S. P. Martin and M. T. Vaughn, Phys. Rev. D **50**, 2282 (1994).
[31] B. C. Allanach, A. Dedes, and H. K. Dreiner, Phys. Rev. D **60**, 056002 (1999).
[32] L. J. Hall and M. Suzuki, Nucl. Phys. **B231**, 419 (1984).
[33] R. Hempfling, Nucl. Phys. **B478**, 3 (1996).
[34] F. Borzumati, Y. Grossman, E. Nardi, and Y. Nir, Phys. Lett. B **384**, 123 (1996).
[35] M. Hirsch, M. A. Diaz, W. Porod, J. C. Romao, and J. W. F. Valle, Phys. Rev. D **62**, 113008 (2000).
[36] B. C. Allanach and C. H. Kom, J. High Energy Phys. 04 (2008) 081.
[37] H. K. Dreiner, J. Soo Kim, and M. Thormeier, arXiv:0711.4315.
[38] J. R. Ellis, J. S. Hagelin, D. V. Nanopoulos, K. A. Olive, and M. Srednicki, Nucl. Phys. **B238**, 453 (1984).
[39] A. H. Chamseddine, R. Arnowitt, and P. Nath, Phys. Rev. Lett. **49**, 970 (1982).
[40] R. Barbieri, S. Ferrara, and C. A. Savoy, Phys. Lett. **119B**, 343 (1982).
[41] L. J. Hall, J. D. Lykken, and S. Weinberg, Phys. Rev. D **27**, 2359 (1983).
[42] S. K. Soni and H. A. Weldon, Phys. Lett. **126B**, 215 (1983).
[43] L. E. Ibáñez and G. G. Ross, Phys. Lett. **110B**, 215 (1982).
[44] L. E. Ibáñez, C. Lopez, and C. Munoz, Nucl. Phys. **B256**, 218 (1985).

[45] A. G. Akeroyd, M. A. Diaz, J. Ferrandis, M. A. Garcia-Jareno, and J. W. F. Valle, Nucl. Phys. **B529**, 3 (1998).
[46] A. de Gouvea, A. Friedland, and H. Murayama, Phys. Rev. D **59**, 095008 (1999).
[47] A. G. Akeroyd, C. Liu, and J.-H. Song, Phys. Rev. D **65**, 015008 (2001).
[48] A. Bartl, M. Hirsch, T. Kernreiter, W. Porod, and J. W. F. Valle, J. High Energy Phys. 11 (2003) 005.
[49] B. C. Allanach *et al.*, arXiv:0710.2034.
[50] M. A. Bernhardt, H. K. Dreiner, S. Grab, and P. Richardson, Phys. Rev. D **78**, 015016 (2008).
[51] C. H. Kom, Cambridge, Ph.D. Thesis.
[52] H. K. Dreiner, P. Richardson, and M. H. Seymour, Phys. Rev. D **63**, 055008 (2001).
[53] H. K. Dreiner, P. Richardson, and M. H. Seymour, arXiv: hep-ph/0001224.
[54] H. K. Dreiner, P. Richardson, and M. H. Seymour, arXiv: hep-ph/9903419.
[55] G. Moreau, E. Perez, and G. Polesello, Nucl. Phys. **B604**, 3 (2001).
[56] F. Deliot, G. Moreau, and C. Royon, Eur. Phys. J. C **19**, 155 (2001).
[57] M. Chemtob, Prog. Part. Nucl. Phys. **54**, 71 (2005).
[58] H. K. Dreiner, M. Krämer, and B. O'Leary, Phys. Rev. D **75**, 114016 (2007).
[59] K. Agashe and M. Graesser, Phys. Rev. D **54**, 4445 (1996).
[60] S. Dimopoulos and L. J. Hall, Phys. Lett. B **207**, 210 (1988).
[61] S. Dimopoulos, R. Esmailzadeh, L. J. Hall, and G. D. Starkman, Phys. Rev. D **41**, 2099 (1990).
[62] B. C. Allanach, M. Guchait, and K. Sridhar, Phys. Lett. B **586**, 373 (2004).
[63] V. M. Abazov *et al.* (D0), Phys. Rev. Lett. **89**, 261801 (2002).
[64] V. M. Abazov *et al.* (D0), Phys. Rev. Lett. **97**, 111801 (2006).
[65] D. Choudhury, S. Majhi, and V. Ravindran, Nucl. Phys. **B660**, 343 (2003).
[66] L. L. Yang, C. S. Li, J. J. Liu, and Q. Li, Phys. Rev. D **72**, 074026 (2005).
[67] H. K. Dreiner, S. Grab, M. Krämer, and M. K. Trenkel, Phys. Rev. D **75**, 035003 (2007).
[68] Y.-Q. Chen, T. Han, and Z.-G. Si, J. High Energy Phys. 05 (2007) 068.
[69] F. Borzumati, J.-L. Kneur, and N. Polonsky, Phys. Rev. D **60**, 115011 (1999).
[70] E. Accomando *et al.*, arXiv:hep-ph/0608079.
[71] A. Belyaev, M.-H. Genest, C. Leroy, and R. R. Mehdiyev, J. High Energy Phys. 09 (2004) 012.
[72] M. Drees and S. P. Martin, arXiv:hep-ph/9504324.
[73] J. F. Gunion and H. E. Haber, Nucl. Phys. **B272**, 1 (1986).
[74] T. Aaltonen *et al.* (CDF Collaboration), Phys. Rev. Lett. **100**, 101802 (2008).
[75] E. Barberio *et al.* (Heavy Flavor Averaging Group (HFAG)), arXiv:0704.3575.
[76] G. W. Bennett *et al.* (Muon G-2 Collaboration), Phys. Rev. D **73**, 072003 (2006).
[77] J. P. Miller, E. de Rafael, and B. L. Roberts, Rep. Prog. Phys. **70**, 795 (2007).
[78] D. Stöckinger, arXiv:0710.2429.
[79] R. Barate *et al.* (LEP Working Group for Higgs boson searches), Phys. Lett. B **565**, 61 (2003).
[80] J. R. Ellis, G. Gelmini, C. Jarlskog, G. G. Ross, and J. W. F. Valle, Phys. Lett. **150B**, 142 (1985).
[81] B. de Carlos and P. L. White, Phys. Rev. D **54**, 3427 (1996).
[82] E. Nardi, Phys. Rev. D **55**, 5772 (1997).
[83] D. N. Spergel *et al.* (WMAP Collaboration), Astrophys. J. Suppl. Ser. **148**, 175 (2003).
[84] M. Colless *et al.*, arXiv:astro-ph/0306581.
[85] B. C. Allanach *et al.*, Eur. Phys. J. C **25**, 113 (2002).
[86] S. Kraml, http://cern.ch/kraml/comparison/.
[87] B. C. Allanach, S. Kraml, and W. Porod, J. High Energy Phys. 03 (2003) 016.
[88] G. Belanger, S. Kraml, and A. Pukhov, Phys. Rev. D **72**, 015003 (2005).
[89] B. C. Allanach, Comput. Phys. Commun. **143**, 305 (2002).
[90] In B_3 SUSY models, Eq. (2.15) is in general modified by additional sneutrino vacuum expectation values v_i. But $v_i \ll v$ in order to be consistent with neutrino masses. We therefore neglect v_i in Eq. (2.15).
[91] V. D. Barger, G. F. Giudice, and T. Han, Phys. Rev. D **40**, 2987 (1989).
[92] Tan β will increase $(\mathbf{Y}_D)$ and $(\mathbf{Y}_E)$, cf. Eqs. (2.13), (2.14), and (2.15). Thus, for tan $\beta \gtrsim 30$, the ordering of the parameters can change to $(\mathbf{Y}_D)^2_{33} > (\mathbf{Y}_E)^2_{33} > g_1^2$.
[93] Note that the charm Yukawa coupling $(\mathbf{Y}_U)_{22}$ is roughly equal to the tau Yukawa coupling $(\mathbf{Y}_E)_{33}$ if tan $\beta = \mathcal{O}(1)$. We have neglected the charm Yukawa coupling, because we assume that tan $\beta = \mathcal{O}(10)$.
[94] In the case of $j = k = 3$, only 8 equations need to be solved. But this implies that the slepton has to be produced by parton quarks of the third generation, which is strongly suppressed due to their negligible parton density.
[95] W. H. Press *et al.*, *Numerical Recipes in C++* (Cambridge University Press, Cambridge, England, 2002), 2nd ed..
[96] B. C. Allanach and M. A. Bernhardt (unpublished).
[97] J. Butterworth and H. K. Dreiner, Nucl. Phys. **B397**, 3 (1993).
[98] H. K. Dreiner and P. Morawitz, Nucl. Phys. **B428**, 31 (1994).
[99] E. A. Baltz and P. Gondolo, Phys. Rev. D **57**, 2969 (1998).
[100] P. Richardson, arXiv:hep-ph/0101105.
[101] F. E. Paige, S. D. Protopopescu, H. Baer, and X. Tata, arXiv:hep-ph/0312045.
[102] G. Corcella *et al.*, J. High Energy Phys. 01 (2001) 010.
[103] G. Corcella *et al.*, arXiv:hep-ph/0210213.
[104] S. Moretti, K. Odagiri, P. Richardson, M. H. Seymour, and B. R. Webber, J. High Energy Phys. 04 (2002) 028.
[105] The version of HERWIG used in this paper was written by Peter Richardson and is available upon request.
[106] In Ref. [9], specific benchmark scenarios with a $\tilde{\tau}_1$ LSP were proposed. We do not consider them here because even the weakest bounds on λ' assuming down-type quark mixing are at the order of $\mathcal{O}(10^{-3})$ for which the rate of resonant slepton production is suppressed.